BIOPHYSICAL APPROACHES FOR MODULATING NEURAL DIFFERENTIATION

by

Alp Özgün

B. S., in Biomedical Engineering, Başkent University, 2012

MSc, in Materials Science and Nanotechnology, Bilkent University, 2014

Submitted to the Institute of Biomedical Engineering

in partial fulfillment of the requirements

for the degree of

Doctor

of

Philosophy

Boğaziçi University

2021

ACKNOWLEDGMENTS

I cannot overstate my gratitude to my PhD advisor Dr. Bora Garipcan, who did not hesitate to guide and support me through hardship, in every way possible.

I greatly appreciate all my friends who transformed the lab environment into an embracing and welcoming home for me. You made these years worth more than any academic output.

My special thanks to my family for always being there, especially my little brother and my biggest ally, Bilal Emre Özgün.

The studies in this thesis were supported by funds from the Scientific and Research Council of Turkey (TUBITAK) (grant numbers 117Z864, 118649) and Boğaziçi University Research Fund (grant number 6701).

ACADEMIC ETHICS AND INTEGRITY STATEMENT

I, Alp Özgün, hereby certify that I am aware of the Academic Ethics and Integrity Policy issued by the Council of Higher Education (YÖK) and I fully acknowledge all the consequences due to its violation by plagiarism or any other way.

Name :

Signature:

Date:

ABSTRACT

BIOPHYSICAL APPROACHES FOR MODULATING NEURAL DIFFERENTIATION

Neural differentiation of stem cells is central to regenerative strategies towards neurodegenerative diseases. The vast majority of literature shows chemical, biochemical and genetic approaches to control and utilize intrinsic or extrinsic stem cells for neural regeneration. However, biophysical factors are also able to regulate stem cell fate with some added advantages. They can be administered to organisms completely non-invasively or used as an integral part of *in vitro* models. Effects of substrate stiffness and electromagnetic fields on neural differentiation are reported in the literature but common for both is a lack of understanding how these biophysical factors interact with cells. The overarching goal of this thesis is to reveal new clues about the effect mechanism of these factors on neural differentiation. Towards this end, three different in vitro neural differentiation models were used in a mechanistic investigation. In the first segment, the results highlight a novel, integrin-independent and biomimetic mechanosensitivity of human neuroblastoma differentiation, along with new caveats attached to using this in vitro biological model. The following segments on electromagnetic fields reveal an unprecedented finding where zinc ions rush into the cells during chronic exposure to 50 Hz electromagnetic field and facilitate other, previously known effects of electromagnetic fields. Moreover, two different ion channels were associated with these effects, for the first time in the literature. Overall, the output of this thesis identifies three new key players for sensing biophysical factors during neural differentiation that will substantially contribute to future efforts towards their utilization in neural regeneration research.

Keywords: Mechanotransduction, extremely low frequency electromagnetic fields, neural differentiation, calcium influx, NMDA receptor, zinc, TRP channels.

ÖZET

NÖRAL FARKLILAŞMAYI ETKİLEMEYE YÖNELİK BİYOFİZİKSEL YAKLAŞIMLAR

Kök hücrelerin nöral farklılaşması, nörodejeneratif hastalıklara yaklaşım stratejileri için merkezi önem arz etmektedir. Literatürde kök hücrelerin nöral rejenerasyon amacıyla kontrol edilmesine yönelik kimyasal, biyokimyasal ve genetik yöntemler gösterilmektedir. Ancak biyofiziksel faktörler de, kök hücre kaderini ek avantajlar sağlayarak değiştirebilmektedir. Bunlar organizmalara girişimsel olmayan yöntemlerle uygulanabilmekte veya *in vitro* modellerin bir parçası olarak kullanılabilmektedir. Substrat sertliği ve elektromanyetik alanların nöral farklılaşmaya olan etkilerinden, literatürde bahsedilmektedir ancak bu ikisi için ortak olan nokta, bu biyofiziksel faktörlerin hücrelerle nasıl etkileştiğinin bilinmemesidir. Bu tezin kapsayıcı hedefi, bu faktörlerin nöral farklılaşmaya olan etkilerinin mekanizmaları ile ilgili bulgular ortaya çıkarmaktır. Buna yönelik olarak üç farklı *in vitro* nöral farklılaşma modeli kullanılmıştır. İlk bölümde sonuçlar, insan nöroblastoma farklılaşmasının integrinden bağımsız ve biyomimetik mekano-hassas boyutunu ortaya çıkarmakta ve bu *in vitro* biyolojik model ile ilgili dikkat edilmesi gereken yeni yönleri vurgulamaktadır. Devam eden bölümler, 50 Hz elektromanyetik alana kronik maruziyet sırasında çinko iyonlarının hücre içine alındığı ve elektromanyetik alanların daha önce bilinen diğer etkilerine olanak sağladığı, yeni bir bulguyu ortaya koymaktadır. Ayrıca literatürde ilk kez iki farklı iyon kanalı bu etkilerle ilişkilendirilmiştir. Sonuç olarak, bu tezin çıktıları, nöral farklılaşma sırasında biyofiziksel faktörleri algılamada üç yeni anahtar oyuncuyu tanımlamaktadır. Bunlar, nöral rejenerasyon araştırmalarında biyofiziksel faktörlerin kullanımına yönelik gelecekteki çabalara önemli ölçüde katkıda bulunacaktır.

Anahtar Sözcükler: Mekanoiletim, çok düşük frekanslı elektromanyetik alanlar, nöral farklılaşma, kalsiyum girişi, NMDA reseptörü, çinko, TRP kanalları.

TABLE OF CONTENTS

LIST OF FIGURES

LIST OF SYMBOLS

$CaCl_2$	Calcium Chloride
Ca^{2+}	Calcium Ions
G	Gauss
g	gram
Hz	Hertz
k	kilo
KCl	Potassium Chloride
KH_2PO_4	Monobasic Potassium Phosphate
L	Liter
M	Molar
$marker^{+}$	positive for the marker
$marker^{-}$	negative for the marker
m	milli
$MgCl_2$	Magnesium Chloride
Mg^{2+}	Magnesium Ions
N	Newton
NaCl	Sodium Chloride
Pa	Pascal
R_D	Resolution Metric
T	Tesla
V	Volt
$ZnCl_2$	Zinc Chloride
Zn^{2+}	Zinc Ions
$^{\circ}C$	degree Celsius
μ	micro

LIST OF ABBREVIATIONS

2-APB	2-Aminoethoxydiphenyl borate
BDNF	Brain derived neurotrophic factor
BM-MSC	Bone marrow-derived mesenchymal stem cell
BSA	Bovine serum albumin
CREB	Cyclic AMP-responsive element-binding protein
DAPI	4,6-diamidino-2-phenylindole
EGFR	Epidermal growth factor receptor
ELF	Extremely low frequency
EMF	Electromagntic field
ER	Endoplasmic reticulum
hNPC	Human neural progenitor cell
ICP-MS	Inductively coupled plasma mass spectrometry
MSC	Mesenchymal stem cell
RA	Retinoic acid
SOCE	Store-operated Ca^{2+} entry
TCP	Tissue culture plate
VEGF	Vascular endothelial growth factor

1. INTRODUCTION

The field of science where theories and techniques of physics are applied to find solutions to biological problems, is called biophysics. This highly multidisciplinary area brings together such fields as structural analyses of biomolecules, computational biology, biomechanics, biomolecular motion, neural networks and medical imaging [1]. From the perspective of biomedical engineering, perhaps the most prominent aspect of biophysics is its importance in biomaterials and bioengineering. The design criteria of implants, *in vitro* models and any other bioengineered platform should account for the fact that cells sense and respond to physical stimuli in their environment [2]. This phenomenon becomes even more important considering the fact that differentiation of stem cells into different lineages is highly responsive to biophysical factors, since stem cell fate is central in most disease and regeneration studies [3]. Hydrostatic pressure, shear stress, matrix elasticity, topography, applied forces and electromagnetic fields (EMFs) are among currently known biophysical factors that affect stem cell differentiation [4].

It is known that hydrostatic pressure of *in vivo* stem cell niches can be highly indicative of healthy and pathological states of related tissues [5,6]. Shear stress-response is another well-characterized biophysical cue that influences stem cell fate. When pluripotent stem cells were pre-differentiated to express vascular endothelial growth factor receptor, these cells to fluid shear stress results in their differentiation into endothelial phenotype [7,8]. When the shear stress is applied directly to pluripotent stem cells without a pre-differentiation protocol, it induces expression of cardiovascular specific markers [9]. Compressive stress on the other hand, when applied to mesenchymal stem cells (MSCs), increases chondrogenic markers and synthesis of cartilage-specific extracellular matrix (ECM) components, both *in vitro* and *in vivo* [10–12]. It is important to realize the biomimetic implications of stem cell responses to these biophysical cues. The fact that cardiovascular endothelial cells are under constant effect of shear stress from blood flow and hyaline cartilage in joints endure dynamic loading of day-to-day physical activity implicate that stem cell responses to these biophysical cues

are due to their innate ability to respond to biophysical aspects of their environment during different stages of life. On the other hand, some cell types interact with their biophysical environments in more unpredictable ways. For instance, subjecting MSCs to visible light in the red region (647 nm) induces osteogenic differentiation [13] which cannot be explained by biomimetic responses. *In vitro* cell substrates with specific topographies at the nanoscale can also influence proliferation and differentiation rates of different types of stem cells [14,15], revealing a whole another field of bioengineering which can manipulate cell behavior by optimizing surface topographies at the micro- and nanoscale.

1.1 Motivation

Substrate stiffness and EMF are biophysical factors that can provide fate-altering stimuli to stem cells and they constitute the main subjects of this thesis [16,17]. Many studies demonstrate different effects of these stimuli on a wide array of biological models. However, the exact mechanism of effect for both of these stimuli remain unknown, especially for EMFs. Knowledge about the underlying mechanisms of observed phenomena is the primary requirement for understanding and utilizing them properly. Revealing how cells "feel" the stiffness of their substrate and other mechanical properties of their environment is a cornerstone in designing better bioengineering platforms where cells are interacted with materials. Understanding the mechanistic underpinnings of cell mechanosensitivity can enable predictions of stem cell behavior in novel environments and prove vital in many regenerative medicine applications. Furthermore, this information can present opportunities for new treatment options and molecular targets for the ever-growing list of diseases where extracellular mechanical properties are found to be involved.

EMFs in low frequency ranges are able to penetrate into live tissues without significant loss or distortion [18]. Firstly, this makes them an excellent candidate for providing stimulus to deep tissues without invasive procedures. The main problem here is that many variables are available with low frequency EMFs such as frequency,

intensity and exposure duration which create an endless number of combinations along with different cell phenotypes, resulting in an extremely wide spectrum of observed effects. A meaningful utilization of these effects will require knowing the precise interactions of EMFs with biomolecules so that biological outcomes can be predicted and EMF parameters can be tuned accordingly.

1.2 Objectives and Outline

The overarching goal of this thesis is to reveal information about how mechanical and electromagnetic stimuli interact with stem cells during neural differentiation on a molecular level. In three main segments, human neuroblastoma cells, human neural progenitor cells (hNPCs) and bone marrow derived mesenchymal stem cells (BM-MSCs) were used as *in vitro* models towards this goal.

In the first segment, SH-SY5Y human neuroblastoma cells were induced to differentiate into neurons on substrates with different stiffness values. Their neural differentiation parameters were monitored along with markers involved in transducing mechanical information into the cell. The following two segments were dedicated to EMF exposure effects on neural differentiation. Due to the vast amount of data available on EMFs in the extremely low-frequency (ELF) range (0-100 Hz), the most commonly used frequency and intensity parameters in the literature (50 Hz, 1 mT) was used for the sake of comparability. 50 Hz EMF was applied to hNPCs and BM-MSCs during neural differentiation, with a field intensity of 1 mT, in conjunction with a panel of Ca^{2+} channel blockers, a meticulous surveillance of various candidate proteins and intracellular physiological parameters. Specific objectives of this thesis include:

- Delivering a non-exhaustive but comprehensive summary of the literature on mechano-environmental and electromagnetic stimuli on neural differentiation, in order to demonstrate the leading edge of this domain.
- Presenting data to show previously unknown mechano-sensitive aspects of neu-

roblastoma differentiation and discussing mechanistic implications of the results.

- Uncovering new mechanistic clues about EMF exposure effects on differentiation of hNPCs, using 50 Hz, 1 mT field parameters.
- Investigating the ion influx that occurs in BM-MSCs under 50 Hz, 1 mT EMF exposure in search of a definitive ion gateway into the cell.

2. BACKGROUND

2.1 Stem Cells and Neural Differentiation

Cells that are yet to be dedicated to a function within a tissue or an organ, and retain self-renewal properties are termed as stem cells. Even though both embryonic and adult stem cells fit this description, they actually have few similarities and exist on the opposite sides of the stem cell potency spectrum. This spectrum starts with the totipotent stem cells which generally refer to the cells of an early zygote. These cells are not only able to proliferate and differentiate into every cell type, they are able to form an entire organism along with the extra-embryonic structures [19]. Pluripotent cells do not have this capability however, they are able to differentiate into cell types of all three embryonic germ layers, endoderm, mesoderm and ectoderm. Embryonic stem cells are the most prominent example of pluripotent stem cells as well as induced pluripotent stem cells where somatic cells are genetically reprogrammed to achieve pluripotency [20]. Adult stem cells are classified into multipotent, oligopotent and unipotent types as they become more and more dedicated towards a specialized cell type. Multipotent stem cells include neural, mesenchymal and hematopoietic stem cells and these are able to proliferate and commit to different cell types within their germ layers. Differentiation of multipotent stem cells into cell types of other germ layers was shown in the literature but results remain controversial and this does not occur in native stem cell niches [21]. Adult stem cell niches usually constitute a pool of self-renewing cells for maintenance and regeneration of tissues [22].

Neurogenesis is defined as generation of new functional neurons from neural stem cells. It was long thought to be terminated after embryonic and post-natal development [23]. Generation of new neurons and addition of these to existing neural circuitry in an adult organism was first shown in songbirds [24]. Later multipotent adult neural stem cells were discovered and the field of adult neurogenesis gained traction with the usage of bromodeoxyuridine which is a nucleotide analog that allows DNA

lineage tracking [25,26]. Adult neurogenesis was found to occur in almost all mammals including humans [27]. This process is however spatially limited to two regions of the brain: subgranular zone of the dentate gyrus in the hippocampus and subventricular zone of the lateral ventricles. These two neurogenic zones generate new immature neurons with different pathways and these migrate to different destinations within the brain [28]. Disruption of these neurogenic pathways are indicated in neurodegenerative diseases such as Alzheimer's [29] and Parkinson's diseases [30] and suggested as potential targets for therapy strategies.

Type B astrocytes are present in both neurogenic regions and act as migratory neural precursors in cases of injury such as neuron loss or demyelination [31]. They act as adult neural stem cells where they remain proliferative well into adulthood and can differentiate into other neural precursor cell types in the neurogenic zones [32]. These cells are easily isolated from rodent brains and can be easily maintained with typical cell culture chemicals [33].

When neurogenesis is approached from an *in vitro* stem cell standpoint, two obviously available choices seem to be neural stem cells and embryonic stem cells. Even though embryonic stem cells are undoubtedly capable of generating all types of neural tissue cells, shortage of supply for human cells of this type generally restrict these studies to other animal sources [34]. Neural stem cells are a convenient supply for *in vitro* neural differentiation models as they are self-renewing cells committed to neural tissue and are able to generate mature neurons, oligodendrocytes and astrocytes. However, they are not able to differentiate into microglia as these cells are sourced from mesodermal infiltrations into brain during development [35]. *In vitro* maintenance of most neural stem cells include strictly defined, complex serum-free media supplemented with epidermal growth factor (EGF) and fibroblast growth factor (FGF) which keeps the cells in mitotic cycle. Withdrawal of these factors arrest the cell cycle and initiate neural differentiation as cells start displaying morphological, biochemical and electrophysiological hallmarks of neurons [36].

Given the information above, MSCs, which are multipotent stem cells, should

not be able to undergo neuronal differentiation as they are mesoderm derived cells. However, they can be manipulated to undergo a process similar to neural differentiation where they morphologically resemble neurons and are able to display some electrical activity, along with an upregulation of certain neural marker proteins [37, 38]. This is termed trans-differentiation of adult stem cells across germ layers and does not in any way give rise to functional mature neurons [21, 39, 40]. Nevertheless, the process itself is still a valid model for neural differentiation where embryonic and neural stem cells are not available. MSCs are amplified in a conventional, serum-containing medium and transferred to a serum-free medium containing certain chemicals such as forskolin, valproic acid and hydrocortisone. These chemicals are known as cyclic adenosine monophosphate elevating agents and they trigger trans-differentiation through largely unknown mechanisms [41]. Recently it was suggested that these agents work by downregulating the neuron-restrictive silencer factor, a transcription regulator that silences neural genes [42].

2.2 Neuroblastoma as a Neural Differentiation Model

Cell lines isolated from neuroblastoma tumors are convenient models for studying neurons and neuronal differentiation *in vitro* [43]. Studying neuroblastoma cells in culture revealed that retinoic acid (RA) treatment causes differentiation into post-mitotic neuron-like cells, facilitating the discovery of effects of retinoids on the development of the nervous system. During post-natal development of the brain, RA plays an important role in neurite outgrowth and axonal path finding processes [44]. *In vitro* RA treatment to neuroblastoma cells causes degradation of F-box protein Skp-2 leading to cell cycle arrest, halted proliferation and eventually differentiation into neuron-like cells [45, 46]. When these findings were translated to clinical applications, retinoids were found to be a highly effective post-resection treatment for neuroblastoma as well as several other malignancies [47].

SH-SY5Y cell line was isolated in 1970 from a 4-year-old patient with neuroblastoma metastasis to bone marrow [48]. The cells secrete dopamine as well as small

amounts of acetylcholine and noradrenaline. Although they are not fully committed dopaminergic cells, they were used as a model for Parkinson's disease which is characterized by a loss of dopaminergic neurons besides other neurodegeneration and neurotoxicity models [49]. *in vitro* differentiation of this cell line usually involves culturing on a surface coated with an ECM protein (eg. Collagen, laminin, fibronectin) or positively charged molecules (eg. Poly-lysine, poly-ornithine) followed by RA treatment in a serum-free medium [50]. Additionally, combinations of brain derived neurotrophic factor (BDNF), nerve growth factor, insulin-like growth factor-1, purines and staurosporine were also used to induce differentiation [51]. Halted proliferation, change of cell morphology from globular to polarized and neurite outgrowth are accepted as the hallmarks of SH-SY5Y differentiation [47]. Even though the most commonly used method of differentiation is RA treatment alone, absence of growth factors during differentiation was associated with the lack of biochemical markers of differentiation such as FAK activity [50]. FAK is an enzyme that strengthens focal adhesion by activating integrins [52]. Integrin-dependent morphology changes and cell migration requires FAK activity, which only occurs after phosphorylation [53]. The differentiation protocol optimized by Encinas et. al. [54] where RA and BDNF are used in conjunction is one of the most well-characterized differentiation processes in the literature which results in both morphological and biochemical differentiation marked by increased expression of neuron-specific markers such as GAP 43, MAP2, Tau and neurofilaments.

SH-SY5Y cells are known to express and deploy voltage gated ion channels in the plasma membrane [55]. Using whole-cell patch clamp technique [56], it was shown that inward currents are primarily through tetrodotoxin-sensitive sodium channels while outward currents occurred via tetraethyl ammonium-sensitive potassium channels. Differentiated and non-differentiated cells varied in terms of current amplitudes and action potential shapes. Non-differentiated cells do not show spontaneous activity and can only be depolarized when membrane potential is clamped to -90 mV [57]. Upon differentiation, cells become more excitable, fire spontaneous action potentials [58] and become mechanically stiffer as an indication of more ion channels on the membrane [47].

SH-SY5Y cells display an unusual morphology when cultured on substrates

softer than conventional tissue culture plates (TCP). As opposed to flat and spread-out cell appearance on TCP, on soft polydimethly siloxane gels they become rounded and cluster together to form ganglion-like structures [59]. Interestingly, in this phenotype, the cells themselves become softer [60] and they get desensitized to amyloid β toxicity [61]. In other studies, they were shown to respond to a wide range of elastic modulus values (0.1-2600 kPa). When cultured on polydimethylsiloxane (PDMS) substrates of elastic modulus values varying between 300-2600 kPa, neurite lengths and the number of focal adhesions increased directly proportional to the substrate elastic modulus [62]. The same trend was repeated when they were cultured on even softer polyacrylamide substrates (0.1 kPa, 1 kPa and 50 kPa) by Lam et. al. [63]. However, this study evaluates differentiation from an oncological point of view and focuses on the effects of substrate stiffness on cell proliferation and morphology rather than neuronal characteristics. Moreover, previous studies used RA as the only differentiation agent which is known to be ineffective for the expression of proteins essential for neuronal function [64].

2.3 Mechanotransduction

Biochemical factors such as small molecules, growth factors and hormones have long been considered to be the primary mechanism of regulation for stem cell functions such as maintenance, proliferation and differentiation [65]. Cells' ability to sense and respond to surrounding mechanical stimuli such as loading, material and topography has been highlighted relatively recently [66]. The most interesting aspect of this phenomenon is the biomimetic responses of stem cells to material stiffness [67]. In this context, stiffness of a material is frequently expressed as elastic modulus of the material in kPa units. Elastic modulus is a measure of how much stress is required to cause elastic deformation of the material, elastic deformation meaning the material restores its original shape upon removal of the stress [68]. In a conventional tensile strength test, elastic modulus is simply the slope of the resulting stress-strain curve. Even though this enables straightforward evaluation of elastic moduli of materials using tensile tests, more advanced methods such as atomic force microscopy scratch tests

and nano-indentation method are able to provide more nuanced data where thin layer coatings or mechanically distinct micro-domains are concerned [69].

Materials fabricated to mechanically represent various tissues or organs show that multipotent stem cells differentiate into the lineages of corresponding tissues. Culturing stem cells on materials matching the average elastic modulus of bone tissue (25-40 kPa) results in osteogenic differentiation while materials that match cartilage tissue (3 kPa) give rise to chondrocytes. The same association was also shown between muscle tissue (8-17 kPa)-myoblasts and pancreas (1.2 kPa)-beta cells [67,70–72]. Mechanosensitivity of neuronal differentiation process has been known as a preference for softer *in vitro* substrates since the discovery of mechanotransductive pathways of stem cell differentiation [67]. Subsequent studies following this finding investigated neuronal differentiation on elastic and stiff substrates using various *in vitro* differentiation models. Materials with elastic moduli between 0.1 and 1 kPa that match an approximate elastic modulus for the whole human brain, induce and enhance neural differentiation, resulting in elevated neural markers and neuritogenesis [63, 73–75]. Moreover, these studies further proved that ECM stiffness gradients are utilized by cells during brain development [76, 77]. Interestingly, literature shows that neuroblastoma cells display a preference for stiff ($\geq$300 kPa) substrates in terms of enhanced neuritogenesis and cell cycle arrest aspects of differentiation [63].

A prerequisite of sensing material stiffness for a cell is adherence, as in attaching to a surface through forming focal adhesions [78]. When adherent cells make contact with a surface, they recognize certain molecules presented on the surface and are able to attach their plasma membranes to the surface through a class of proteins called cell adhesion molecules [79]. This adherence occurs mainly through several anchor points for each cell and is followed by reorganization of the cytoskeleton by using these anchor points as support while the cell assumes its final morphology. The forces exerted on the material at these focal adhesions is thought to be the main feedback a cell receives about the mechanical properties of its environment [80]. The forces exerted to a material by the cell can actually be tracked by a method called traction force microscopy where displacement of fluorescent beads embedded within a transparent

material is monitored during cell activity in order to map the material deformation and calculate stress fields [81].

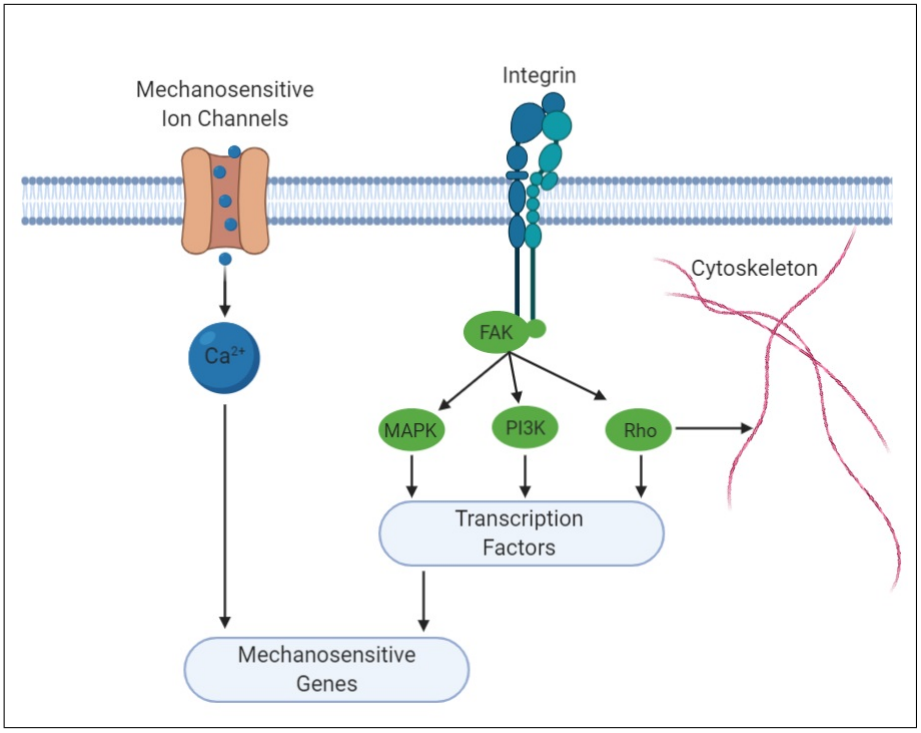

Figure 2.1 Proposed mechanotransduction pathways in the literature. Reproduced with permission from [83] Elsevier, Copyright (2011).

Forces generated at the focal adhesions are considered to be the starting point of mechanosensing, where transmembrane receptor integrins are the major player, as seen in Figure 2.1 [82]. Integrins cluster at the focal adhesion upon formation and recruit focal adhesion kinase (FAK) at the intracellular site [83]. Activation of FAK through phosphorylation is able to start multiple intracellular cascades including MAPK, PI3K and Rho all of which regulate gene expression through transcription factors [84], along with the more direct and rapid pathway of mechanosensitive Ca^{2+} channels [85]. Moreover, integrins are able to interact with the actomyosin cytoskeleton directly and indirectly [86], conveying mechanical messages bi-directionally. This means that integrin-dependent pathways not only influence gene expression and actomyosin cytoskeleton organization, but also controls integrin binding to extracellular ligands, such as ECM epitopes [87]. Majority of findings in this field suggest that integrin-dependent mechanotransduction is the main facilitator of substrate stiffness mediated stem cell differentiation [88, 89].

2.4 Neural Differentiation and EMFs

Electromagnetic spectrum contains all kinds of electromagnetic energy starting from high frequency, high energy gamma rays all the way to low energy, low frequency radio waves and below. Below the frequency of radio waves electric and magnetic components of electromagnetic waves become distinguishable and are usually referred to as electromagnetic fields [90].

Electromagnetic fields within the frequency range of 0-300 Hz are called extremely low frequency (ELF) electromagnetic fields (EMF) and are of very little use to daily human activity such as broadcasting and communications. ELF range is substantially below useful frequencies for communications due to their extremely large wavelengths since transmitting and receiving signals require antennae dimensions correlated with the carrier signal wavelength. This impracticality limits its usage to sending short messages to deeply submerged submarines from expensive facilities with miles-long antennae. Therefore one can jump to the conclusion that humans are not exposed to significant amounts of ELF EMF relative to humans' daily exposure to radio, TV and cellular phone carrier signal frequencies [91]. However, it is safe to say that the world is practically doused in ELF radiation since power wires are used everywhere around humans to carry electricity and moving charges along a wire creates a magnetic field around the wire. Since 50-60 Hz alternating currents (AC) are used to carry electrical power, this means that all power carrying cables are producing 50-60 Hz radiation. Another magnitude that needs to be considered about electromagnetic fields is their strength. EMF strength units are Tesla (T) and Gauss (G). In this context Tesla unit is more prevalent. For comparison the strongest magnetic field humans can get exposed to in daily life is 1.5 or 3 T from magnetic resonance imaging and standing half a meter away from a house power line exposes to 1.5 μT field intensity at 50 Hz frequency [92].

Long-term exposure to ELF EMF elicits subtle responses from biological systems, which become important in the context of hazards of chronic, occupational exposure of humans [93, 94]. These responses also present potential for useful applications that can be applied noninvasively due to undisturbed penetration of ELF EMFs into

biological structures. However, not enough knowledge exists about the molecular basis of the interactions between ELF EMFs and biological systems to make predictions and form hypotheses.

Research shows that ELF EMFs in the extremely low frequency range affect survival, proliferation and phenotype of cells from different sources in addition to neural differentiation of different stem cell types [95–99]. The vast majority of these studies use weak ELF EMFs with an intensity of 1 mT and 50 Hz frequency, making these parameters ideal for mechanistic approaches due to availability of large amount of data. The most frequently reported molecular events are increased intracellular Ca^{2+} and ROS levels as a result of 50 Hz MF exposure [99–108]. Limited evidence exists about the source of increased oxidative stress [109] but the elevation of intracellular Ca^{2+} is generally attributed to L-type voltage gated Ca^{2+} channels [105, 108, 110–112]. It is important to note that the mentioned studies use a wide variety *in vitro* models and include both excitable and non-excitable cells which makes it hard to pinpoint a clear pathway by pooling their results. For instance, observed effects were traced to L-type Ca^{2+} channels in chromafin cells [102], P/Q, N and R type Ca^{2+} channels in neurons [106] and TRPC1 channels in embryonic neural stem cells [96]. Other efforts at finding ELF EMF-sensitive pathways include identification of ATM-Chk2-p21 pathway activation in a human keratinocyte cell line by 60 Hz MF [113] and ERK1/2 modulation of human osteoblasts by pulsed MFs [114]. Perhaps the most profound mechanistic finding is on the neural-like differentiation of bone marrow-derived mesenchymal stem cells (BM-MSCs) under 50 Hz EMF exposure where the increase in neural marker expression was tied to increased cyclic AMP-responsive element-binding protein (CREB) phosphorylation [115]. Later, this effect was traced back to activation of epidermal growth factor receptor (EGFR)-Akt cascade by 50 Hz MF exposure in BM-MSCs [116] and other models [117]. These were schematized in Figure 2.2. However, further upstream events of EGFR phosphorylation were never investigated in this context.

EGFR pathway is regulated by the Zn^{2+} binding ADAM enzyme family [118]. Other Zn^{2+} binding enzymes such as matrix metalloproteases [119] and Egr1 transcrip-

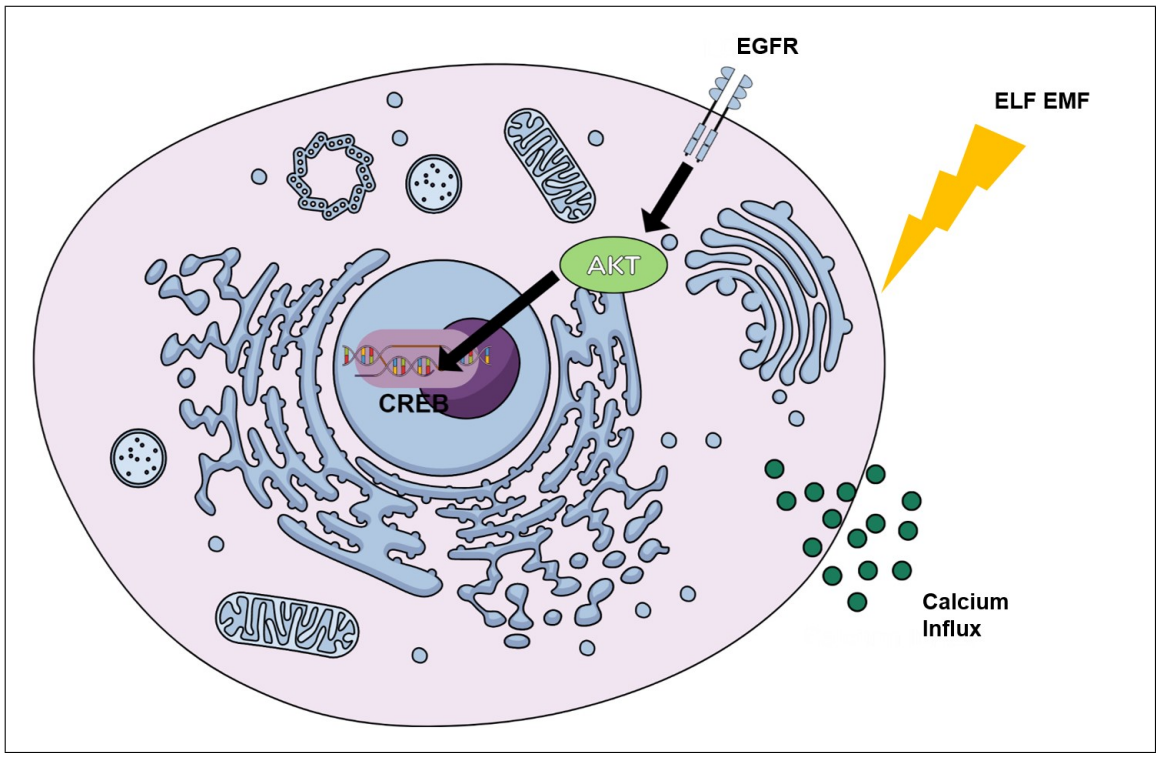

Figure 2.2 Characterized pathways involved in ELF EMF-induced neural differentiation.

tion factor were also reported to be activated in response to 50 Hz EMFs. Furthermore, most commonly used Ca^{2+} probes and chelators have a much higher affinity towards Zn^{2+} [120–122]. Even though free Zn^{2+} concentrations are far smaller than Ca^{2+}, it plays important roles in cell homeostasis and is considered a secondary messenger [123]. Examining the given clues, Zn^{2+} becomes a previously unnoticed candidate worthy of investigation as a player in the effects of ELF EMF exposure.

3. SUBSTRATE STIFFNESS EFFECTS ON SH-SY5Y: THE DICHOTOMY OF MORPHOLOGY AND NEURONAL BEHAVIOR

In this study, it was aimed to test if soft substrates with elastic moduli matching or stiffer than brain ECM (0.1 kPa) have an effect on biochemical and electrophysiological characteristics of SH-SY5Y differentiation. For this purpose, collagen I (Col I) coated polyacrylamide (PA) hydrogel substrates with elastic moduli below 1 kPa (denoted 0.1 kPa), over 1 kPa (denoted 1 kPa) and above 25 kPa (denoted 50 kPa) were prepared and RA - BDNF treatment was used to differentiate SH-SY5Y cells cultured on these substrates, as well as Col I coated TCP surfaces. Data shows that, despite their rounded morphology, cells on softer substrates are more easily excited. Moreover, when substrate stiffness matches brain ECM elastic modulus, TUJ 1 neuronal marker levels increase compared to other soft substrates and TCP. These results present a contradiction between neuronal morphology and behavior of this *in vitro* neuron model and raise more questions about its validity, especially in the context of biomechanical studies.

3.1 Experimental Procedures

All reagents were used as purchased without further processing. Details of each protocol were provided below.

3.1.1 Preparation of PA Hydrogels

GelBond polyacrylamide support films (Lonza) were cut into discs that fit into 48 and 6-well plates (Corning). 40% acrylamide (Merck) and 2% N,N'-methylenebisacrylamide (Merck) solutions were prepared in phosphate buffered saline pH:7.4 (PBS). All solu-

tions were sterilized by passing through 0.2 μm syringe filters and the remaining steps were performed in a sterile laminar flow cabinet. Gel precursor solutions were prepared for achieving 3 types of PA hydrogels with distinct Young's modulus values, initially named A, B and C from soft to stiff. Acrylamide and N,N'-methylenebisacrylamide content of gel precursor solutions were optimized in order to achieve criteria for 0.1 kPa, 1 kPa and 50 kPa groups, respectively. Tetramethylethylenediamine and 200 mM aqueous ammoniumpersulfate solution were added to gel precursors to a final concentration of 3% in order to initiate polymerization. Gel precursors were dropped on sterile plastic petri dish surfaces and covered with GelBond discs, activated side facing the solution. 40μL gel precursor was used per cm^2 of GelBond film area. After being allowed to polymerize at room temperature for 30 minutes, PA hydrogels attached to GelBond discs were gently removed from the petri dishes and placed into well plates.

For Col I immobilization on PA hydrogel surfaces, 25 mg/mL Sulfo-SANPAH solution was prepared in dimethyl sulfoxide (DMSO) and diluted into water to a final concentration of 1 mg/mL. PA hydrogel surfaces were covered with this solution and kept 10 cm away from a 320 nm UV lamp for 15 minutes. After washing twice with dIH2O, 100 μg/mL Col I solution was added on the hydrogels and kept at 4Â°C for 12 hours. Subsequently, Col I solutions were aspirated and PA hydrogels were washed three times with PBS. Col I immobilization density was quantified by staining the samples with Sypro Ruby Protein Gel Stain overnight and washing thoroughly according to manufacturer's instructions. Background samples were incubated in Col I solution without Sulfo-SANPAH modification in order to offset physical binding of protein to surfaces. Fluorescence density was measured with fluorescence microscopy at 450/610 nm excitation/emission. Before cell seeding, PA hydrogels were kept in cell culture medium for 2 hours.

3.1.2 Mechanical Characterization

Gel precursors were polymerized in 24-well plates for mechanical analysis. Cylindrical samples with 3.5 mm height and a diameter of 16 mm were characterized me-

chanically by a Dynamic Mechanical Analyzer (DMA) (TA Instruments Q800). The compression test method was used due to the geometry of the samples. Before tests, precise calibrations of the instrument and clamp were performed. In order to obtain the stress-strain diagram as the output, the DMA controlled force module was selected with the step of force increment of 1 N/min up to 18 N. The thickness of each sample in three groups was determined by the measurement tool of the instrument applying the preloading with the value of 0.0005 N. The diameters of the samples were measured by a sensitive micrometer before loading samples to the instrument. All samples had almost identical dimensions, which eliminated size effect on the results.

3.1.3 Cell Culture and Differentiation

SH-SY5Y cells were cultured in growth medium composed of DMEM-F12 (Biosera) containing 10% FBS (Merck) and 1% penicillin/streptomycin (Biosera). Cells were trypsinized and seeded on substrates with a density of 5x10^4 cells/cm^2 in growth medium. Well plates were coated with Col I for TCP group prior to seeding. After overnight incubation to facilitate cell adhesion on substrates, growth medium was replaced with 1 mL/cm^2 differentiation medium which is serum-free DMEM/F12 supplemented with 5μM retinoic acid and 10 ng/mL brain derived neurotrophic factor. Cells were kept in this medium for 7 days, without light and disturbance.

3.1.4 Immunocytochemistry

Cells were fixed in 4% formaldehyde solution for 10 minutes and permeabilized with 0.5 % saponin treatment. Formaldehyde solutions were prepared and used fresh by dissolving paraformaldehyde in PBS and readjusting pH to 7.4. Both fixative solution and cells were equilibrated to room temperature before the fixation step. Blocking was performed by incubating the cells in 1% Bovine Serum Albumin (BSA) solution containing 22 mg/mL glycine and 0.1% Tween 20 in PBS. Primary antibodies for p-FAK (Santa Cruz, sc-81493) and TUJ1 (Santa Cruz, sc-80005) were diluted 1:100 in 1%

BSA solution and incubated with the cells at 4°C overnight. Negative control cells from all groups were incubated in 1% BSA solution instead. Secondary antibody (Abcam, ab150106) was diluted 1:500 in 1% BSA and incubated with cells, including negative controls, for 2 hours at room temperature. Cytoskeleton was stained using Alexa Fluor 488 conjugated phalloidin and nuclei were counterstained with 4',6-diamidino-2-phenylindole (DAPI). Substrates were washed twice with PBS between each step. Cells were imaged and photographed with fluorescence microscopy (Leica DM IL).

3.1.5 Western Blot

Protein lysates were collected from cells by incubating substrates in Laemmli buffer for 10 minutes. Obtained samples were boiled at 95°C and loaded to 4-10% discontinuous PA gels. Protein bands were resolved at 200 V (Bio-Rad, Mini Protean) and transferred to PVDF membranes (Bio-Rad, Transblot Turbo). Before antibody probing, protein bands were stained with ponceau S dye in order to confirm that loading control actin to total protein ratio remains the same between groups. Membranes were blocked with 1% BSA in tris-buffered saline containing 0.1% Tween 20 (TBST). Target bands were probed with primary antibodies for p-FAK and TUJ1 (Santa Cruz, sc-81493 and sc-80005 respectively) diluted 1:1000 in 1% BSA/TBST solution. After overnight incubation in primary antibody, Horseradish peroxidase conjugated secondary antibody (Abcam, ab6789), diluted 1:1000, was incubated with the membranes for 2 hours. Membranes were washed with TBST and bands were visualized using a 3,3',5,5'-tetramethylbenzidine based colorimetric substrate (Thermo).

3.1.6 Calcium Imaging

Fluo 8-AM was dissolved in DMSO and diluted to a final concentration of 5 μM in Hank's buffered salt solution (HBSS). Cells were incubated in this medium for 30 minutes at 37°C for dye loading and de-esterification. Loaded cells were washed with HBSS and further incubated in dye-free HBSS at 37°C for 30 minutes in order

to restore electrophysiological equilibrium. Substrates were transferred to fluorescence microscope (Zeiss, Axio) and images were recorded at 100 frames per second before, during and after isosmotic application of KCl to a final concentration of 45 mM. Image series from each recording were analyzed by creating a standard deviation stack using ImageJ in order to identify responsive cells. Fluorescence of each responsive cell was analyzed over time as a different region of interest relative to background fluorescence. The cells that display a fluorescence increase 1.2 times over basal signal was considered responsive [124].

3.1.7 Statistical Analysis

Statistical variance between samples was computed with GraphPad Prism software. Sample distribution normality was tested using Shapiro-Wilk test followed by one-way ANOVA for parametric samples and Kruskal-Wallis test for non-parametric samples. All data are presented as mean $\mp$ standard deviation of three independent experiments. Calculated p values that are lower than 0.05 were considered significant and denoted as * for $p<0.05$, ** for $p<0.01$ and **** for $p<0,0001$.

3.2 Results

3.2.1 PA Hydrogel Preparation

PA hydrogel formulations were optimized until determined Young's modulus criteria were met for all experimental groups. Criteria were determined for these groups to obtain two groups of hydrogels that are under 1 kPa and between 1 kPa and 2 kPa thus, achieving two subtly different categories with only one soft enough to match neural tissue ECM stiffness. A third, considerably stiffer group was added to emphasize stiffness dependence of the effects. DMA results were displayed as in Figure 3.1, show 0.43 ∓ 0.27 kPa, 1.40 ∓ 0.32 kPa and 45.39 ∓ 16.14 kPa elastic moduli for these groups, respectively.

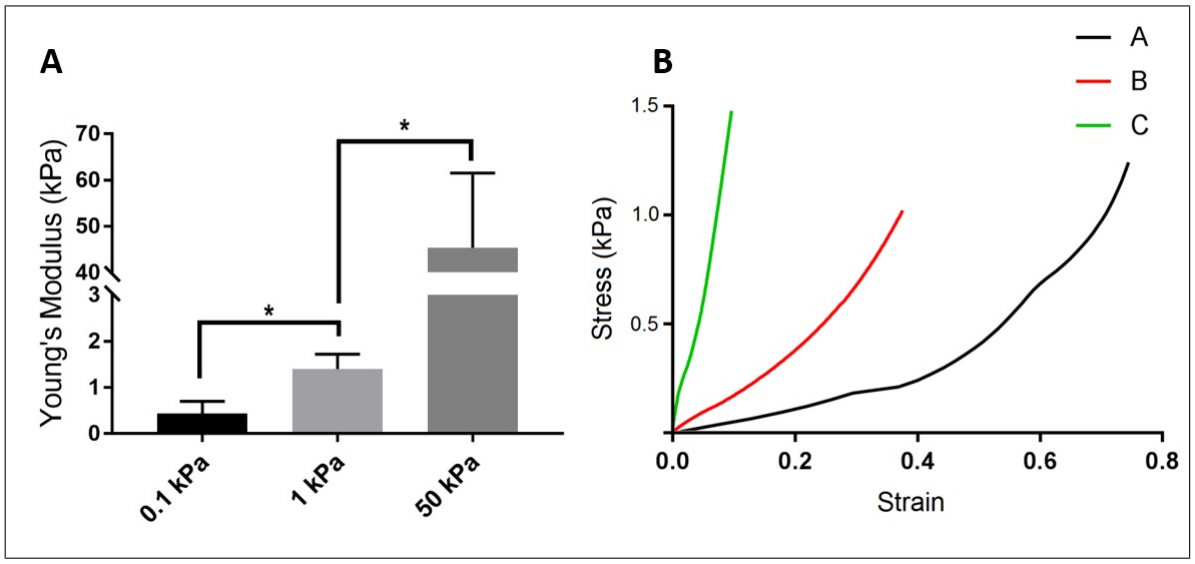

Figure 3.1 A) Dynamic mechanical analysis results and B) sample stress/strain curves of PA hydrogels prepared with formulations for three different stiffness values (0.1-50 kPa).

3.2.2 Cell Culture and Differentiation

24 hours after seeding, cells on 0.1 kPa and 1 kPa surfaces display spherical, clustered morphology, as opposed to typical spiny shapes of SH-SY5Y cells on TCP surface (Figure 3.2). 50 kPa group also has the same morphology with TCP group at this stage. Even though clustered cells resemble floating cells that failed to attach, they remain on the surface after rigorous washing with medium and PBS. Red particles attached to PA hydrogel surfaces are also visible in bright field images. These form after sulfo-SANPAH/UV treatment of the surface and stay visible thereafter. Differentiation causes neurite growth and shrinkage of cell bodies in TCP and 50 kPa groups. No neurite outgrowth was observed in 0.1 kPa and 1 kPa groups and their morphology did not change at all after 7 days of differentiation.

3.2.3 Immunostaining and Western Blot

Immunocytochemistry results show that all cells in all groups are positive for both p-FAK and TUJ 1 as Figure 3.3 and 3.4 suggest. Cytoskeletons appear as long

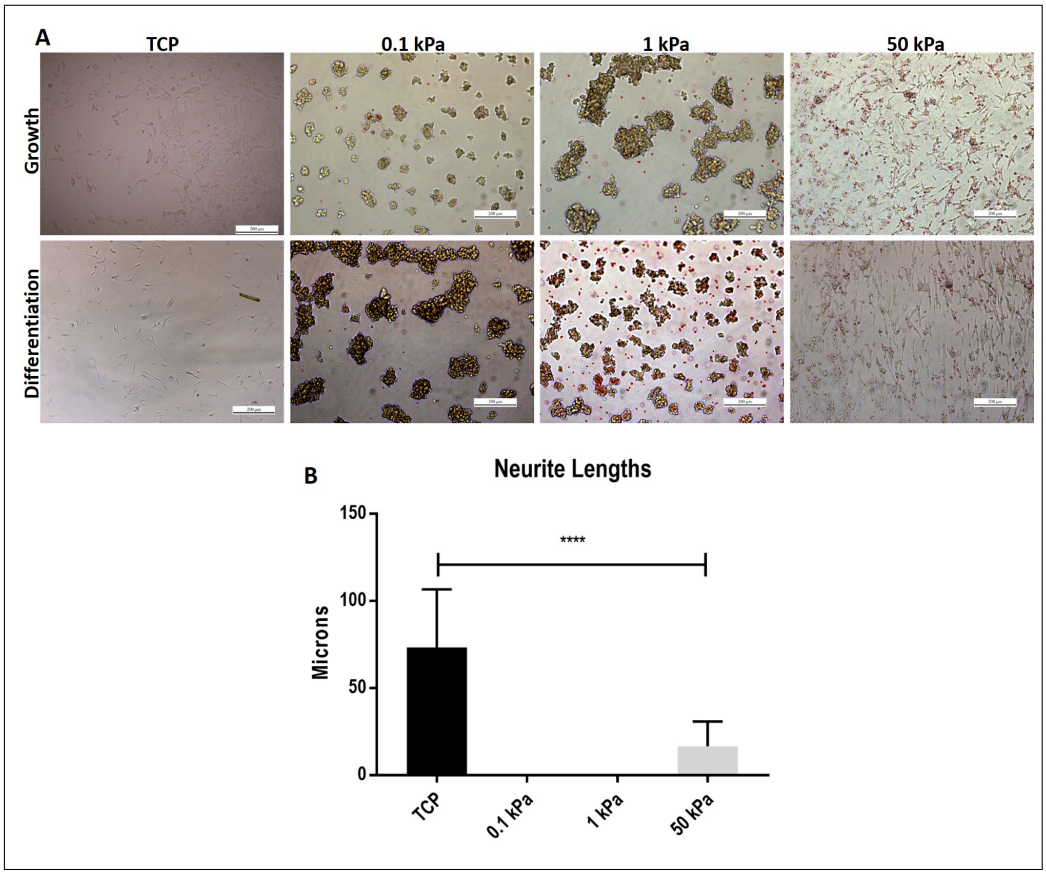

Figure 3.2 A) Bright field microscopy images of SH-SY5Y neuroblastoma cells seeded and differentiated on PA hydrogels (0.1-50 kPa). Growth group shows cell morphology 24 hours after seeding and differentiation group images were taken after 7 days in differentiation medium. Scale bar 200 microns. B) Mean neurite lengths measured from cells differentiated on each substrate.

filaments in the TCP group whereas PA hydrogel groups display short F-actin filaments with more intense fluorescence.

Cell morphologies in 50 kPa group appear different than bright field images. They now resemble 0.1 kPa and 1 kPa groups having lost their neurites indicating that formaldehyde fixation destroyed their focal adhesions to the surface.

In order to verify that this result is not a consequence of a problem with the fixation protocol or differences in protein immobilization, L929 fibroblasts were seeded on TCP and 50 kPa PA hydrogel surfaces. Figure 3.5 shows that these cells adhere to both surfaces at 24 hours and show similar morphology before and after fixation. Also seen in Fig 3.5, Col I density on PA hydrogel surfaces are statistically indistinguishable

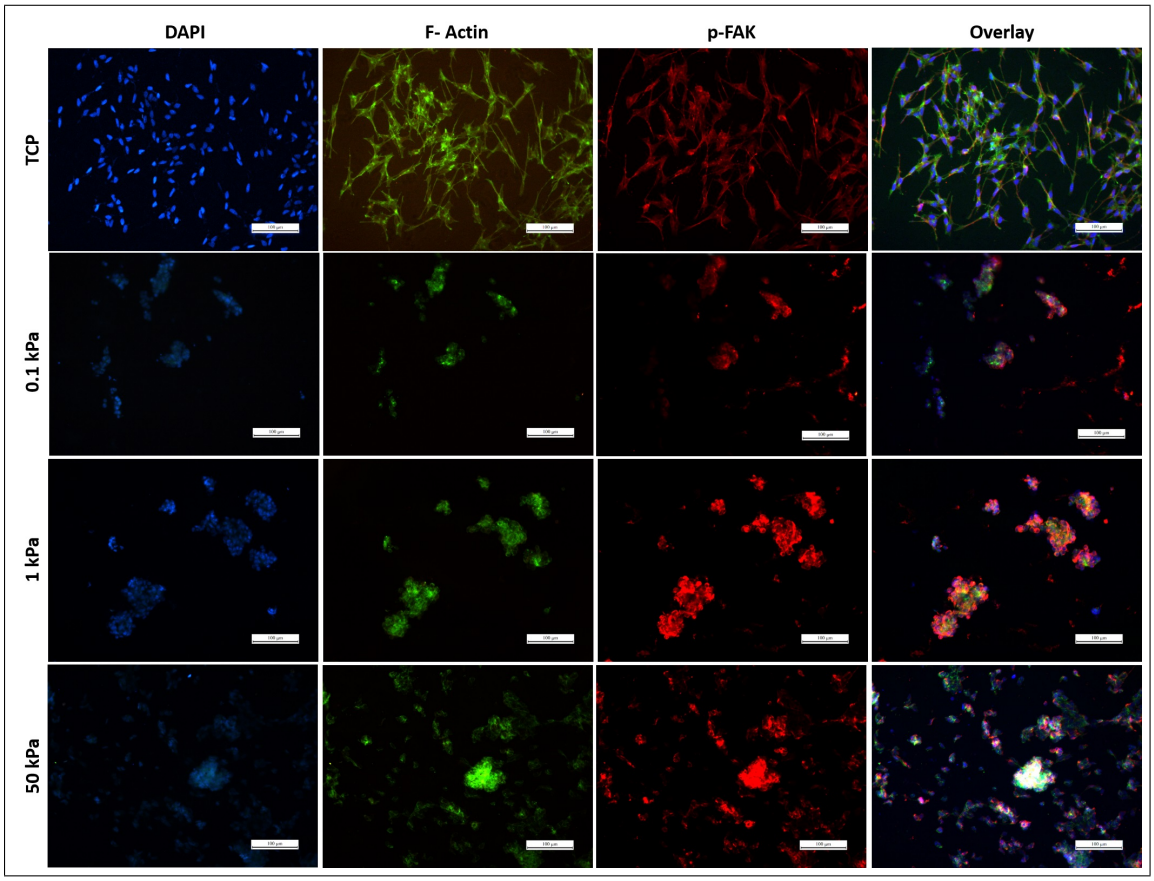

Figure 3.3 Fluorescence microscopy images of SH-SY5Y neuroblastoma cells differentiated for 7 days on PA hydrogels (0.1-50 kPa) and immunostained for p-FAK. Cytoskeleton was stained green with an F-actin dye and nuclei were counterstained with DAPI. Scale bar 100 microns.

between groups (0.1-50 kPa).

Although the number of cells expressing TUJ 1 and p-FAK remain the same between groups, when total abundance of these proteins are probed with western blot, some differences arise. Levels of TUJ1 in 0.1 kPa group are significantly higher, compared to other groups as seen in Figure 3.6. There is an apparent variation between p-FAK levels of cells differentiated on different substrates, which seems to follow surface stiffness however; these differences are not large enough to become statistically significant.

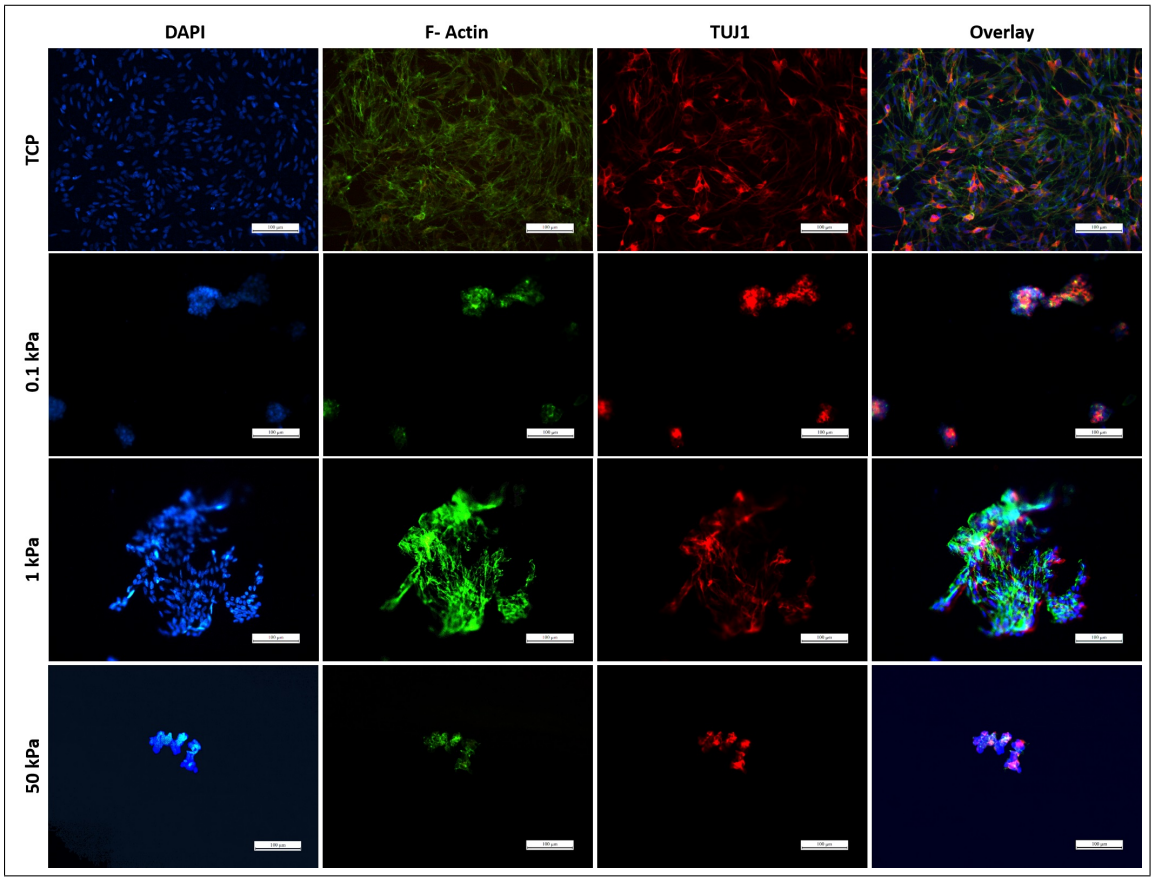

Figure 3.4 Fluorescence microscopy images of neuroblastoma SH-SY5Y cells differentiated 7 days on PA hydrogels (0.1-50 kPa) and immunostained for TUJ 1. Cytoskeleton was stained green with an F-actin dye and nuclei were counterstained with DAPI. Scale bar 100 microns.

3.2.4 Calcium Imaging

When cells were loaded with the Ca^{2+} indicator, their responses to stimulation varied substantially between groups. Figure 3.7 shows that, the percentage of responsive cells becomes higher as substrates get softer from 50 kPa to 0.1 kPa. Interestingly, a linear trend (p=0.0002, R square=0.9925) was found between means of these percentage values as substrate stiffness changes.

3.3 Discussion

Mechanosensitivity of neuronal differentiation process has been known as a preference for softer *in vitro* substrates since the discovery of mechanotransductive path-

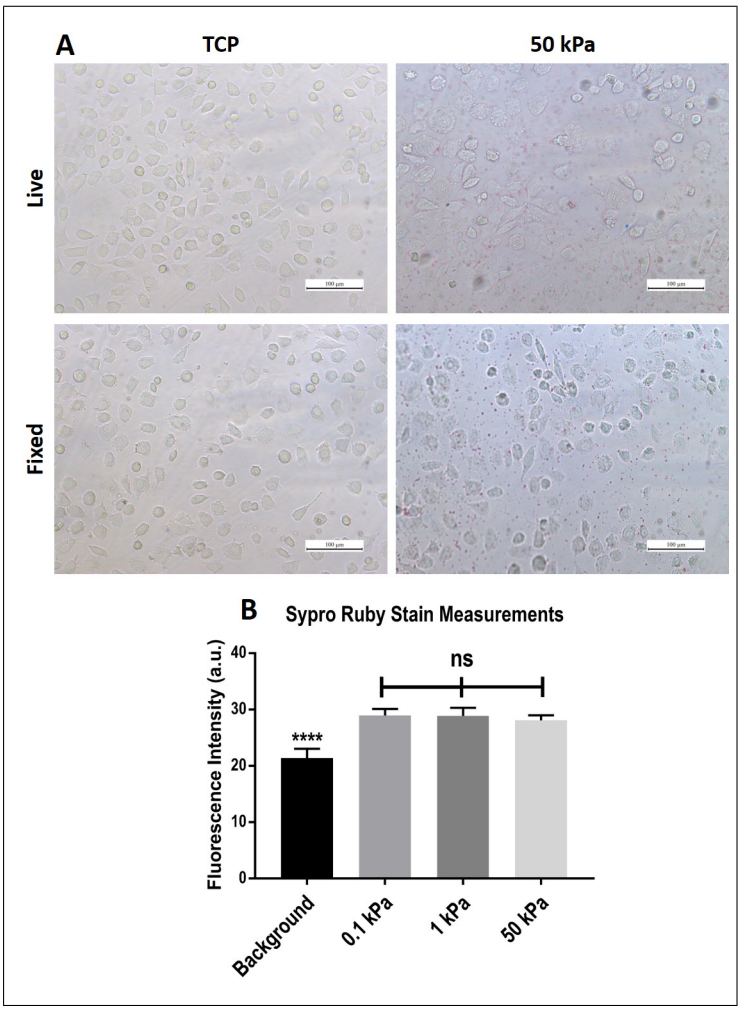

Figure 3.5 A) Bright field microscopy images of L929 fibroblasts on PA hydrogels (0.1-50 kPa) and B) Col I coverage densities on PA hydrogels measured by Sypro Ruby Protein Stain fluorescence. Scale bar 100 microns.

ways of stem cell differentiation [67]. Subsequent studies following this finding investigated neuronal differentiation on elastic and stiff substrates using various *in vitro* differentiation models [63, 73, 74]. Interestingly, literature shows that neuroblastoma cells display a preference for stiff ($\geq$300 kPa) substrates in terms of enhanced neuritogenesis and cell cycle arrest aspects of differentiation [63]. Here, polystyrene TCP as a stiff substrate ($\sim$GPa) [125] was compared to PA hydrogels in three groups with decreasing Young's modulus values in order to characterize the effect of substrate stiffness on electrophysiological and biochemical aspects of differentiation. Mechanical analyses show the lack of overlap between Young's modulus values of groups to ensure subtly different but statistically distinct mechanical properties of experimental groups.

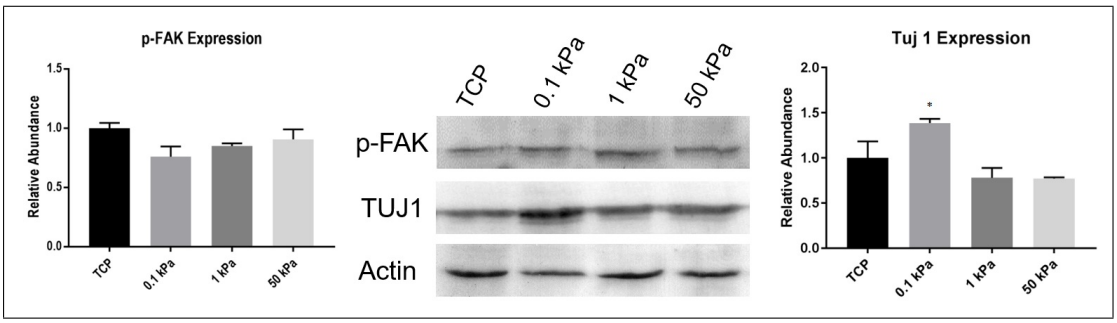

Figure 3.6 Western blot analyses of p-FAK and TUJ 1 in neuroblastoma SH-SY5Y cells differentiated on different substrates (0.1-50 kPa) along with sample membrane images.

Mimicking elastic properties of native ECM to manipulate cell fate *in vitro* is an interesting concept where differentiation occurs in the favor of cell types found in native microenvironments that elastically match the stiffness of the substrate [67, 72]. In this study, ganglion-like structures previously reported in the literature [60, 63] were reproduced on 0.1 kPa and 1 kPa surfaces. However, increasing surface rigidity to 50 kPa restored the cell morphology displayed on TCP surfaces indicating that ganglion formation requires matrix elasticity to be comparable to neural tissue ECM. Interestingly, on 50 kPa surfaces cells display shapes identical to TCP group after seeding but upon differentiation, neurite outgrowth occurs to a much lesser extent, confirming previous studies [62].

Activity of FAK is important for the adhesion and migration of neuronal cells and abundance of p-FAK is regarded as a parameter for confirmation of differentiation in SH-SY5Y cells [50].Results from p-FAK immunofluorescence show reactivity in all cells on all 0.1 kPa, 1 kPa and 50 kPa surfaces. Images captured with identical microscopy parameters appear to exhibit similar levels of fluorescence signal between groups. A lack of significant difference between groups in western blot analysis of p-FAK verifies this observation. F-actin, co-stained for observation of the cytoskeleton alongside target markers, reveals that morphology of 50 kPa group changed drastically upon formaldehyde fixation, marked by the loss of neurites observed in bright-field microscopy of live cells. Destruction of neurites by slight cell volume changes caused by fixative solution can be interpreted as an indication of weakened focal adhesions on soft substrates, as recently reported in the literature [60], arising through mechanisms

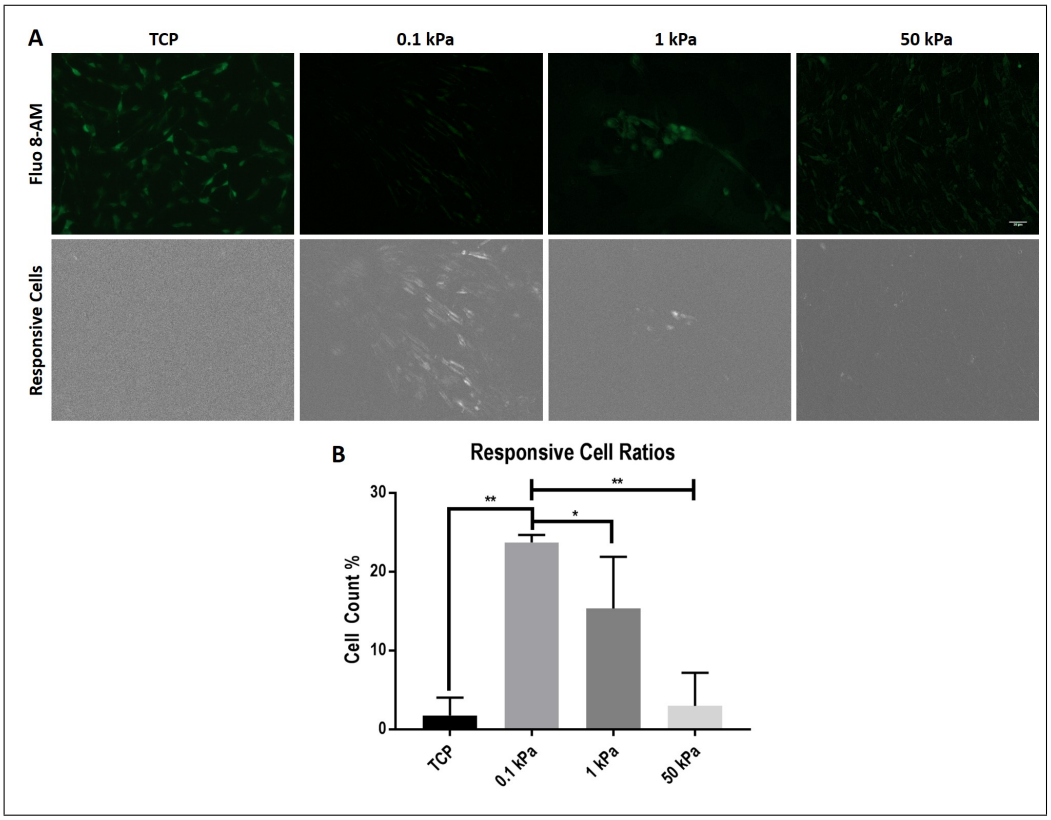

Figure 3.7 A) Example calcium signals and calcium responses revealed by creating standard deviation Z-projects from calcium imaging videos. B) Percentages of SH-SY5Y cells responsive to stimulus after being differentiated on substrates with different elastic moduli (0.1-50 kPa).

independent from FAK activity. The possibility of this finding being the result of a procedural problem was ruled out by showing that the same fixation protocol does not change the morphology of a different cell line. Moreover, equal protein density on samples with different stiffness values was verified to show that the weakening of focal adhesions was not due to lack of Col I on the surface.

In previous studies, formation of ganglion-like structures and absence neurite outgrowth on soft substrates were evaluated as morphological hallmarks of inefficient neuronal differentiation or lack thereof [63]. In this thesis, data shows that biochemical and electrophysiological characteristics of neuronal behavior develop independently from morphological parameters. Even though all cells are positive for TUJ1 neuronal marker regardless of substrate stiffness, western blot results show a significant increase in total TUJ1 levels only when substrate elasticity matches native brain tissue [67]. The fact that TUJ1 abundance does not change in response to substrate stiffness above 1

kPa posits that biochemical differentiation of SH-SY5Y cells is enhanced by mechanical biomimicry of neural tissue.

Interestingly, calcium response to stimulation demonstrates a near perfect dependence on substrate stiffness. Even though hippocampal neurons were previously reported to show a preference for stiff substrates in terms of neuronal activity [73], SH-SY5Y cells seem to respond at higher rates when cultured on softer substrates. This can be attributed to an increase in expression or membrane deployment of calcium channels as matrix stiffness decreases.

4. ELF EMF INDUCES HUMAN NEURONAL DIFFERENTIATION THROUGH NMDA RECEPTOR ACTIVATION

In this study, possible involvement of NMDA receptors in the effect of ELF EMFs on neuronal differentiation was explored. Differentiating hNPCs were exposed to 50 Hz, 1 mT ELF EMF, as these are the most commonly utilized parameters for neuronal differentiation in the literature [126]. It is demonstrated that 50 Hz ELF EMF exposure during neuronal differentiation enhances the levels of neuronal markers, c-fos and neurite outgrowth. These effects are completely reversed by treatment with an NMDA receptor antagonist, revealing a heavy NMDA receptor dependence. Implications and possible processes that lead to these findings are discussed. Current results provide a robust affirmation to the hypothesis as all previously reported effects of ELF EMF exposure are eliminated by memantine treatment. Furthermore, hNPCs have never been used as an *in vitro* model of neuronal differentiation for ELF EMF studies before, which makes the findings more relevant to ELF EMF effects on human neural tissue.

4.1 Experimental Procedures

All reagents were used as purchased without further processing. Details of each protocol were provided below.

4.1.1 Cell Culture and ELF EMF Exposure

hNPCs were gifted by Prof. Leo A. Behie (University of Calgary, Calgary, Canada). Cells were isolated from the telencephalon of a 10 week post-conception fetus under strict ethical guidelines established and approved by the Conjoint Health

Research Ethics Board (CHREB, University of Calgary, Canada; ID: E-18786) guidelines [127]. Frozen neurospheres of hNPCs were thawed at 37°C and transferred into a T25 cell culture flask (Nunc) in PPRF-h2 medium [128]. Two days later, neurospheres were dissociated by trituration and re-seeded in fresh PPRF-h2 medium to allow reformation and growth of spheres. During 14 days of growth, 40% of medium was refreshed every other day. For differentiation, neurospheres were enzymatically dissociated (0.25% Trypsin-EDTA, GIBCO) and transferred to differentiation medium consisting of Neurobasal A (Thermo Fisher) supplemented with 10 ng/mL bFGF (Sigma Aldrich), 2% B-27 supplement (Thermo Fisher) and 0.5% Glutamax (Thermo Fisher). Cells (monolayer) were then seeded on poly-D-lysine (100 μg/mL, Sigma Aldrich) and laminin (10 μg/mL, Sigma Aldrich) coated coverslips at a density of $2x10^4$ cells/cm^2 [129]. Intact neurospheres were directly added on coated coverslips without dissociation. Intact neurosphere seeding was only performed for an initial visual evaluation. All other experiments are performed with monolayer cells obtained from dissociated neurospheres. Memantine treatment was performed by dissolving memantine (Sigma Aldrich) in PBS and adding to media at a final concentration of 2 μM [130]. Final vehicle concentration in media was kept below 0.01%. Sham and ELF EMF group plates were placed in different incubators at 37°C under 5% CO2 atmosphere. Cells were allowed to differentiate for 5 days under control (sham exposure) or continuous 50 Hz, 1.0 mT ELF EMF exposure conditions. ELF EMF exposure was provided by a Helmholtz coil pair placed inside the cell culture incubator [115]. 50 Hz sinusoidal signal was obtained by attenuating power line signal through a variac and fed to the coils to maintain a 1.0 mT root mean square field intensity which was measured by an EMF spectrum analyzer (Aaronia NF-5035).

4.1.2 Immunocytochemistry

hNPCs were washed with PBS and fixed with 4% formaldehyde (Sigma Aldrich) solution in PBS for 10 min and permeabilized with PBS containing 0.1% Triton X-100 (Sigma Aldrich). After blocking non-specific binding sites with 10% fetal calf serum (Thermo Fisher) in PBS for 1.0 h at room temperature, coverslips were incubated

in primary antibodies against MAP2 (mature neuronal marker Abcam, mouse, 1:500), doublecortin (DCX) (Santa Cruz, goat, 1:300) or c-fos (Abcam, Rabbit, 1:300) for 2.0 h at room temperature. Corresponding secondary antibodies (Abcam, 1:500) conjugated with either Alexa Fluor 488 or Alexa Fluor 594 were sequentially added and incubated at room temperature for 1.0 h. Nuclei were counterstained with DAPI for 10 min and micrographs were taken with fluorescence microscopy (Olympus BX-61) [131].

4.1.3 Western Blot

Differentiated hNPCs were harvested into ice cold RIPA buffer and protein concentrations were estimated by Bradford assay (Bio-Rad). Lysates were diluted in 2X Laemmli buffer before use. 4-10% discontinuous polyacrylamide (Sigma Aldrich) gels were cast and proteins were resolved under 120 V (Bio-Rad, Mini Protean). Protein bands were transferred (Bio-Rad, Transblot Turbo) to PVDF membranes (Millipore). Membranes were probed with primary antibodies against MAP2 (Abcam, mouse, 1:500), Tuj1 (Santa Cruz, mouse, 1:1000) and DCX (Abcam, rabbit, 1:500) at 4°C, overnight. Corresponding horseradish peroxidase conjugated secondary antibodies (Abcam, 1:2000) were added on membranes and incubated for 1.0 h at room temperature. Bands were visualized by adding 3,3',5,5'-Tetramethylbenzidine chromogenic substrate (Thermo Fisher) on the membranes. Scanned membranes were quantified by ImageJ software.

4.1.4 Quantification of Micrographs

ImageJ software was used for analyzing immunostaining micrographs. Marker positive cells were counted by applying a threshold to each of at least 25 images from each group, so that only marker expressing cells remain on the foreground. DAPI stained total nuclei and cells positive for each marker were counted manually. NeuronJ, an ImageJ plugin, [132] was used to manually mark and measure the length of all $MAP2^{+}$ neurites from at least 20 images from each group. Micrographs from c-fos

immunostaining experiment were converted to grayscale and each MAP2$^+$ cell was manually selected with region of interest tool for making mean gray value measurements for c-fos. Background measurements were subtracted from intensity values of each cell. At least 19 images were analyzed for each group.

4.1.5 Statistical Analysis

Statistical significance of ELF EMF exposure and memantine treatment effects were tested by two-way ANOVA followed by Tukey's HSD post-hoc test using Graphpad Prism software. One-way ANOVA was used for cell counts where memantine treatment was not performed. All data presented as mean $\mp$ SEM of three independent experiments. Calculated p values that are lower than 0.05 were considered significant and denoted as * for $p<0.05$, ** for $p<0.01$ and n.d. for differences that are not significant. Exact p values are given in the text.

4.2 Results

The effect of ELF EMF exposure on neuronal differentiation of hNPCs was first assessed by immunostaining for early (DCX, marker for immature neurons) and mature neurons (MAP2). Intact neurospheres and dissociated cells were differentiated for qualitative and quantitative evaluation respectively, under sham and continuous ELF EMF (50 Hz, 1.0 mT) exposure conditions. hNPCs differentiated as a monolayer resulted in a population of 52.5% $\mp$ 2.9 DCX$^+$ and 57.0% $\mp$1.82 MAP2$^+$ cells. Total number of cells and populations did not differ ($p=0.899$ and 0.507 for DCX and MAP2, respectively) under ELF EMF exposure conditions (Figure 4.1a). Neurospheres attached to the culture surface upon induction of differentiation and cells started to migrate. A gradual decline of DCX$^+$ was observed as cells migrated away from the neurosphere core; whereas ELF EMF group showed an abrupt reduction in DCX$^+$ cells immediately outside the neurosphere boundary (Figure 4.1c). This finding was expressed as the profile of DCX signal intensity plotted against the distance from neurosphere core

(Figure 4.1b). DCX signal at the neurosphere center decays to 10% of initial values within 259 ∓ 47 μm distance in ELF EMF group, compared to 482 ∓ 30 μm in sham group (p=0.040).

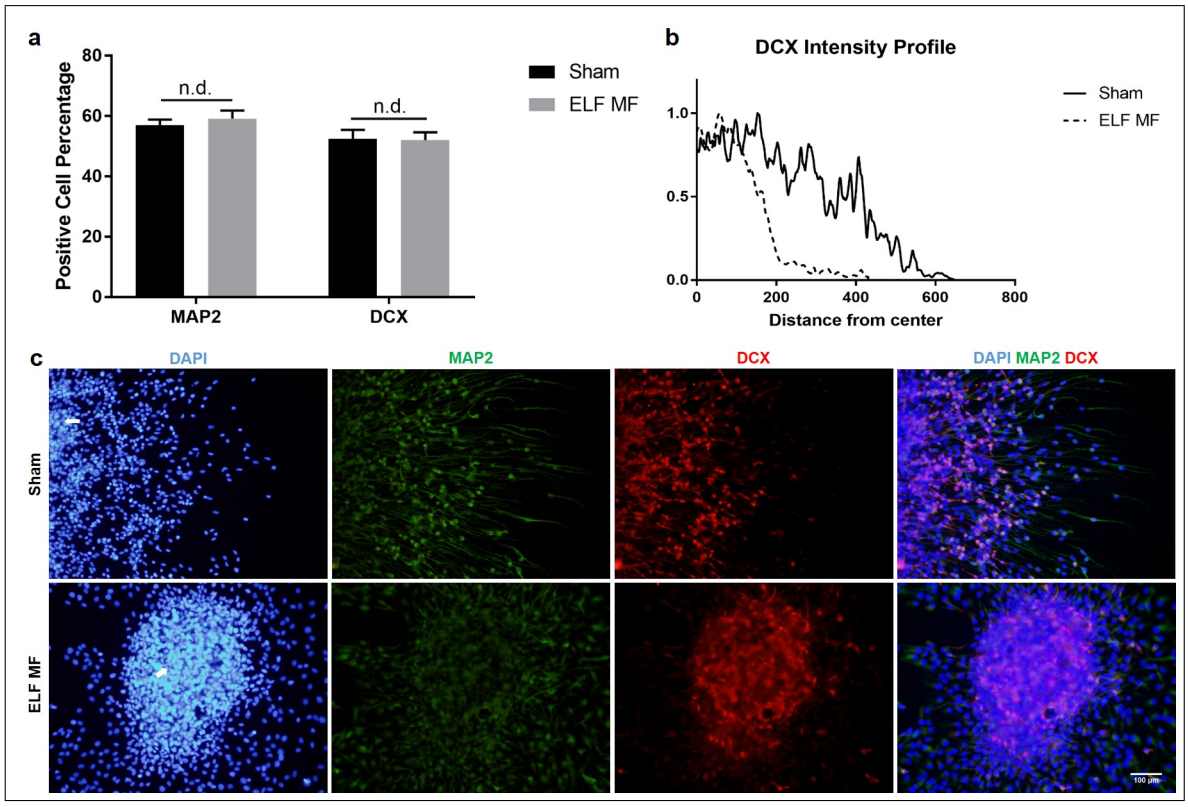

Figure 4.1 Assessment of immature (DCX^+) and mature ($MAP2^+$) neuron populations under 50 Hz, 1.0 mT ELF EMF exposure a) Quantification of $MAP2^+$ and DCX^+ neurons obtained from monolayer cultures as a percentage of total nuclei under sham and ELF EMF conditions b) Sample DCX intensity profiles of images taken from neurons differentiated as intact neurospheres as a function of distance from the neurosphere center c) DCX (red) and MAP2 (green) immunofluorescence images of neurons differentiated as intact neurospheres where initial neurosphere cores are marked with white arrows on DAPI (blue) stained nuclei; scale bar 100 μm for all micrographs in panel. Data presented as the mean ∓ SEM of three independent experiments; n.d. non-significant according to one-way ANOVA.

Neuronal differentiation of monolayer cultures was further evaluated through total abundances of neuronal markers, comparatively estimated by western blots. Overall results of two-way ANOVA reveal significant effect of ELF EMF on all tested markers (p=0.003, 0.013 and 0.042 for TUJ1, MAP2 and DCX, respectively) but no significant effect of memantine treatment alone (p=0.434, 0.193 and 0.762 for TUJ1, MAP2 and DCX, respectively). ELF EMF exposure resulted in significantly (p=0.016 and p=0.003 respectively) elevated total levels of mature neuronal markers MAP2 and TUJ1 (Figure

4.2a and b) while early neuron and migration marker DCX levels showed a sharp drop (p=0.009) compared to sham exposure (Figure 4.2c). Blocking NMDA receptors, by treating the cells with uncompetitive channel antagonist memantine, neutralized the effects of ELF EMF exposure on all three markers. Memantine treatment alone had little to no effect on (p=0.323, 0.859 and 0.076 for TUJ1, MAP2 and DCX, respectively) the abundance of markers (Figure 4.2a-c).

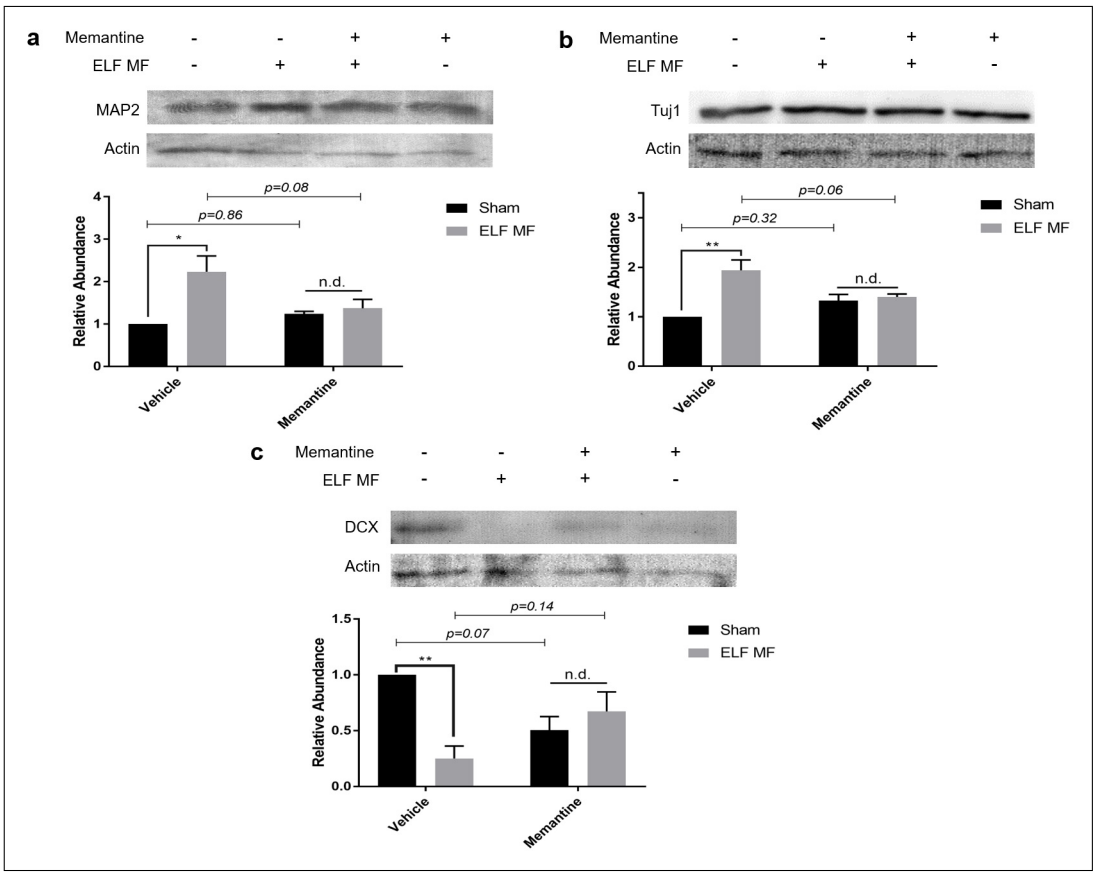

Figure 4.2 Western blot analysis of early and mature neuron markers in monolayer cultures under ELF EMF exposure and memantine treatment conditions. Representative blot images and densitometry analyses of a) MAP2, b) TUJ1 and c) DCX as normalized to actin expression. Data presented as the mean ∓ SEM of three independent experiments; **p<0.01, *p<0.05, n.d. non-significant according to Tukey's HSD post-hoc test.

ELF EMF also enhanced morphological maturation of neurons in an NMDA receptor dependent manner. Overall two-way ANOVA results show significant effects for both ELF EMF (p=0.007) and memantine treatment (p<0.001) on neurite lengths of mature neurites. $MAP2^+$ neurites were significantly longer (p=0.004) in cells differentiated under exposure while memantine treated cells were not (p=0.949) affected by ELF EMF (Figure 4.3) according to post-hoc analysis.

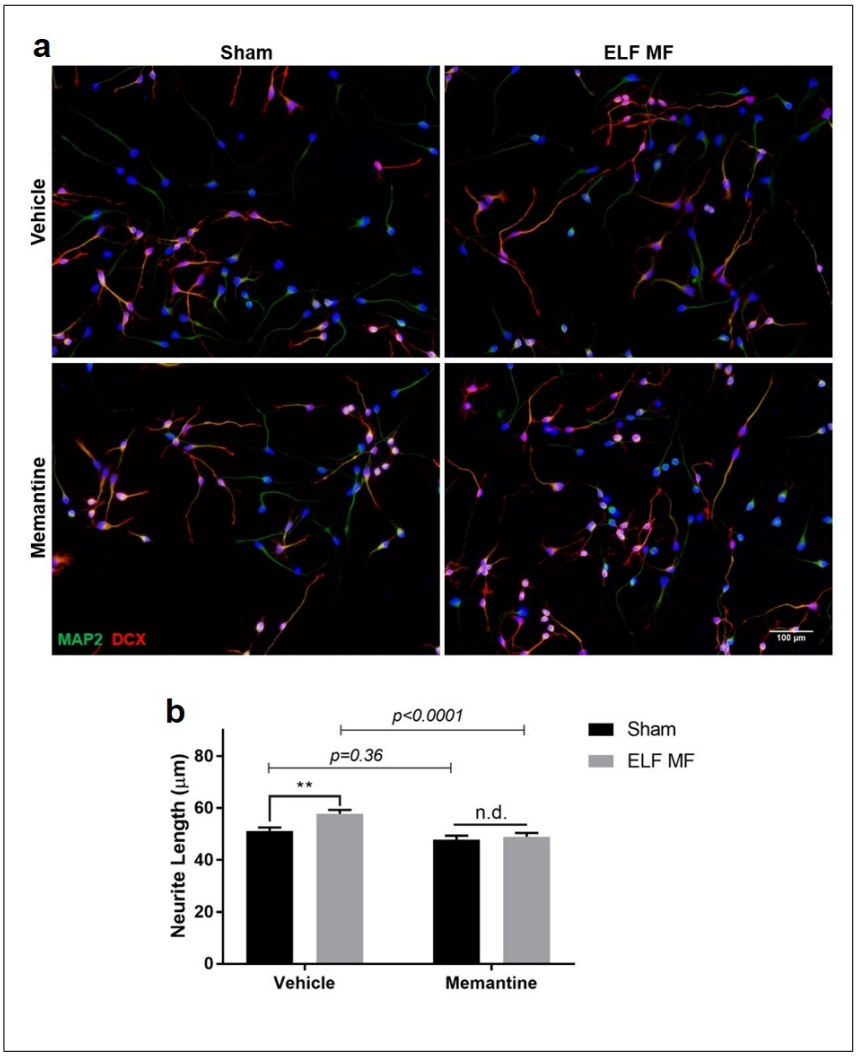

Figure 4.3 Effect of ELF EMF exposure and memantine treatment on neurite lengths of hNPCs differentiated as monolayers. a) Representative images of MAP2 (green) and DCX (red) immunostained cells along with b) neurite length analysis of each group. Data presented as the mean ∓ SEM of three independent experiments; **p<0.01, n.d. non-significant according to Tukey's HSD post-hoc test.

An NMDA receptor based effect of ELF EMF on neuronal activity was also identified by measuring c-fos levels in $MAP2^+$ cells. Mean c-fos fluorescence signal intensities within these cells were heightened by both ELF EMF exposure (p=0.007) and memantine treatment (p<0.001) according to overall two-way ANOVA test. Presence of memantine alone produced a sharp increase (p<0.001) in c-fos levels but also eliminated the effect of ELF EMF exposure as signal intensities were indistinguishable between sham and ELF EMF groups under memantine treatment (Figure 4.4).

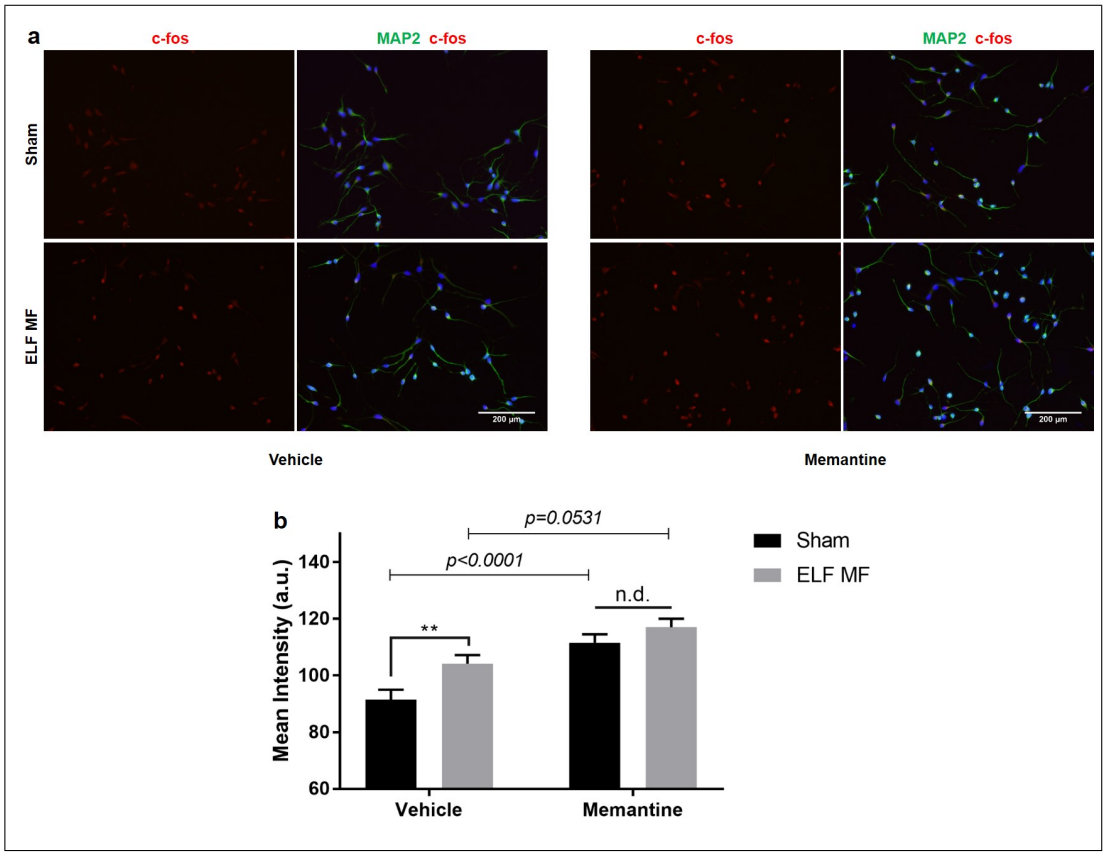

Figure 4.4 Effect of ELF EMF exposure and memantine treatment on c-fos expression of hNPCs differentiated as monolayers. a) Representative images of hNPCs immunostained for MAP2 (green) and c-fos (red) given with b) quantification analysis of c-fos signal intensity from $MAP2^+$ cells. Data presented as the mean ∓ SEM of three independent experiments; **p<0.01, n.d. non-significant according to Tukey's HSD post-hoc test.

4.3 Discussion

Despite concerns about biological effects of chronic exposure and its epidemiological association with neurodegenerative diseases, [133] ELF EMFs may hold potential for new, non-invasive intervention options for diseases of neural tissues due to their unperturbed penetration into biological media and subtle but promising effects on the molecular level. These include ameliorating cognitive symptoms of Alzheimer's disease [134, 135] and attenuating tau phosphorylation which is one of the molecular hallmarks of Alzheimer disease [136]. They are known to drive different stem cell populations towards neural differentiation when applied at 50 Hz, *in vitro* [96,115,116,137] and *in vivo* [138], even in the absence of differentiation factors [115]. Although investigations into neural differentiation effects almost exclusively use 50 Hz fields, other

parameters such as field intensity, exposure duration, exposure intervals and signal waveform vary widely between studies as well as their obtained results [126]. Optimizing these parameters with a purposefully designed waveform to elicit a selective, well-defined and useful molecular response constitutes the ultimate goal of this field. Pinpointing exact interaction mechanisms of ELF EMF with neural tissue is therefore the major milestone towards this target.

In the pursuit of these mechanisms, the most commonly identified effect is the elevation of intracellular Ca^{2+} concentration *in vivo* and *in vitro* [99–106]. Concomitant effects of Ca^{2+} influx such as increased expression levels of c-fos and c-myc [101] along with augmented protein kinase A, protein kinase C and calcineurin activities [104] were also determined. Enhancement of neuronal differentiation under ELF EMF exposure was previously linked to cyclic AMP-responsive element-binding protein CREB phosphorylation which could be traced back to EGFR activation through Akt signaling in the upstream [116]. Still, no proven rationale exists about the starting point of the cascade that is triggered by the ELF EMF exposure and results in neuronal differentiation. Considering the clues mentioned above, the NMDA receptor, a relatively unexplored candidate as a Ca^{2+} gateway in this field, may be the starting point in the cascade. NMDA receptor activation results in Ca^{2+} influx and activation of Ca^{2+} dependent pathways [139] which agrees with the elevation of intracellular Ca^{2+} under ELF EMF exposure. It is also known that NMDA receptor activation heavily promotes neuronal differentiation [140], as NMDA receptor signaling is a major regulator of proliferation and differentiation of neural progenitor cells [141, 142]. The hypothesis is further reinforced by the fact that the aforementioned EGFR-Akt-CREB cascade is stimulated by NMDA receptor activation at multiple points, namely; Akt phosphorylation is known to be triggered by NMDA treatment *in vitro* and EGFR phosphorylation can be enhanced by NMDA receptor activation through upregulation of ADAM10 [143]. Considering the above information, it is tempting to hypothesize NMDA receptors to be the starting point of ELF EMF effects on neural progenitors. Current results provide a robust affirmation to this hypothesis as all previously reported effects of ELF EMF exposure are eliminated by memantine treatment. Furthermore, human neural progenitor cells (hNPCs) have never been used as an *in vitro* model of neuronal differ-

entiation for ELF EMF studies before, which makes the findings more relevant to ELF EMF effects on human neural tissue.

The absence of an effect of ELF EMF on MAP^+ cell population is already expected since neuronal-glial fate is determined by completely different processes which cannot be altered during differentiation after commitment to a cell type [144]. However, intact neurospheres seem to dissipate less efficiently under ELF EMF exposure as they exhibit clearer boundaries with DCX^- cells around them. Since DCX plays an important role in neuronal migration [145], it can be inferred that the rapid loss of DCX expression slows the expansion of differentiating neurospheres. This qualitative observation is also confirmed by western blot data which shows a drastic drop in total DCX levels of monolayer cultures. Intact neurosphere differentiation was performed solely for visualizing purposes and was not repeated for other experiments as they do not allow cell counting for seeding and analysis. Mature neuron marker levels are shown to be enhanced under ELF EMF exposure, which confirms previous reports on different *in vitro* models [96, 116, 146]. Memantine is a use-dependent uncompetitive antagonist of NMDA receptor. It shares a binding site with the Mg^{2+} channel block, meaning glutamate binding and Mg^{2+} block dislodging are both required for memantine activity, which also make it a voltage dependent blocker. After memantine binds to channel opening, the channel can close and trap the molecule inside. This characteristic is shared with other common NMDA receptor blockers such as amantadine, ketamine, MK-801 and phencyclidine [147, 148]. The results demonstrate that blocking NMDA receptors in this manner prevents ELF EMF from enhancing neuronal marker levels as well as restoring early neuron marker DCX to normal levels. These findings create adequate basis to propose that exposure to ELF EMF magnifies NMDA receptor activation which leads to improvement of neuronal differentiation. It can be speculated that ELF EMF may increase channel open probability through effects on the Mg^{2+} block or due to local fluctuations in the trans-membrane potential caused by induced eddy currents. The findings are further reinforced by analyzing two more NMDA receptor facilitated events; c-fos levels [149] and neurite outgrowth [150–152]. An increase in c-fos expression of mature neurons was already expected as a response to the rise in intracellular Ca^{2+} levels which confirms previous studies reporting Ca^{2+}

influx in response to ELF EMF exposure [99–106]. Interestingly, presence of memantine alone also resulted in significant increase in c-fos which is explained by previous findings where memantine administration induced c-fos expression in cortical neurons *in vivo* [153]. Conversely, memantine treated cells exhibited similar levels of c-fos between sham and ELF EMF exposure groups, eliciting that Ca^{2+} influx under exposure is triggered by NMDA receptors. Lastly, it is shown that neurite outgrowth is augmented by ELF EMF exposure, confirming previously reported results [96], which was also shown to be an NMDA receptor mediated effect as displayed by relapsed neurite lengths in memantine treated group.

5. ELF EMF-INDUCED Ca^{2+} INTAKE BY MESENCHYMAL STEM CELLS IS LINKED TO AN ACCOMPANYING Zn^{2+} INFLUX

The aim of this study is to inquire the possible involvement of Zn^{2+} in the EMF effects commonly reported in the literature, with a focus on intracellular cation increase. Using BM-MSCs as a model, the effects on neural marker Tuj1 and ROS levels are first reassessed and then the gateways of cation entry were investigated, through a set of rigorous calcium imaging experiments and a panel of blockers. The results were able to confirm Zn^{2+} as a major player and identify a primary entryway for cations under the effect of 50 Hz EMF exposure.

5.1 Experimental Procedures

All reagents were used as purchased without further processing. Details of each protocol were provided below.

5.1.1 Cell Culture and ELF EMF Exposure

BM-MSC cell lines were purchased from Thermo Fisher and Kocaeli University KOGEM stem cell research and gene therapy center. Cells were propagated in DMEM/F12 medium (Pan biotech) supplemented with 10% fetal bovine serum and used between passage numbers 3 and 6. For the experiments, cells were trypsinized, counted and re-plated at $3x10^3$ cells/cm^2 density, in serum-free medium consisting of DMEM/F12, 5mM KCl, 2μM valproic acid, 10 μM forskolin, 1 μM hydrocortisone and 5 mg/ml insulin. Cells intended for flow cytometry or western blot were plated in 35 mm petri dishes while type I collagen-coated coverslips were used for microscopy experiments. Plates were placed inside the coils of the ELF EMF exposure system within an

incubator set at 37°C and 5% CO2. Sham group plates were placed in another section of the incubator that's been magnetically isolated from the exposure system.

Magnetic field exposure system for cell culture was designed as a set of Helmholtz coils fed by a power amplifier, which in turn is driven by signals from a PC sound card. Helmholtz coils consist of two identical coils that are fixed one radius apart from each other, in order to obtain homogenous field intensity between them. 668 turns of 18 Gauge sheathed copper wire was used in each coil with a radius of 10 cm. This optimized design ensured generation of 50 Hz magnetic fields with up to 2 mT intensity, without increasing the temperature. Using signals from a PC sound card offers a wide variety of waveforms that can be digitally synthesized and played as opposed to standard signal generators. OPA 544 high voltage, high current operational amplifier was used to amplify the signals from the sound card and feed the Helmholtz coils. Amplifier gain was adjusted using a variable feedback resistor to obtain the desired field intensity. Measurements of field intensity were performed using Aaronia NF 5030 electromagnetic field spectrum analyzer, which allowed analysis in a wide frequency domain, instead of single frequency measurements. Finally, the coils were sterilized with 70% ethanol and placed inside the cell culture incubator through a cable port, which was then resealed to prevent gas leakage and contamination. Temperatures of 50 Hz exposure and control groups were regularly checked during experiments using an infrared thermometer.

Cells were kept under 50 Hz, 1mT ELF EMF exposure for 7 days for all experiments. Memantine (4 μM), nifedipine (10 μM), gabapentin (10 μM), ethosuximide (10 μM), 2-aminoethyl diphenylborate (2-APB) (10 μM), N,N,N',N'-Tetrakis(2-pyridylmethyl)ethylenediamine (TPEN) (2 μM) and ZnCl2 (5 μM) were included in the media of corresponding groups.

5.1.2 Western Blot

Protein content of the cells were harvested into cold RIPA buffer by scraping and total protein content was measured using Bradford assay (Bio-Rad). Lysates were diluted into 2X Laemmli buffer before SDS-PAGE. Discontinuous polyacrylamide gels were cast and protein bands were resolved at 120 V (Bio-Rad, Mini Protean). Resolved proteins were transferred to PVDF membranes (Bio-Rad, Transblot Turbo) and the bands were first visualized by incubating the membranes in Ponceau S solution for 2 minutes. After washing the membranes, they were blocked in 5% BSA for 1 hour at room temperature. Target proteins Tuj1 (Santa Cruz, sc80005), NR2A (Santa Cruz, sc515148), Cacna2d1 (Santa Cruz, sc271697) and actin (Santa Cruz, sc58673) were probed by 1:1000 diluted primary antibody incubation for 18 hours at 4°C. Secondary antibody (Santa Cruz, sc516102) was incubated for 1 hour at room temperature and bands were visualized using chromogenic TMB blotting substrate (Thermo Fisher). Membranes were scanned and images were quantified using ImageJ software.

5.1.3 Mitochondrial Membrane Potential Imaging

Mitochondrial membrane potential probe JC-1 was used to detect any changes that may arise in mitochondrial activity. This dye binds to mitochondria in a voltage dependent manner and its bound form red-shifts in emission which enables ratiometric imaging of both free and bound form and accurate voltage evaluation of mitochondrial membrane [154]. JC-1 (Merck) was dissolved in DMSO and diluted into serum-free medium to 10 μg/ml. Cells were incubated in dye solution for 10 minutes and washed with fresh medium 3 times before imaging under fluorescence microscopy with 488 nm excitation. Ratios of red and green emission from the captured images were measured by ImageJ software.

5.1.4 Measurement of Reactive Oxygen Species

A fluorescence based total ROS detection kit (Enzo, ENZ-51011) was used to evaluate changes in intracellular ROS levels. According to kit instructions, the detection reagent was diluted 1:5000 in the provided wash buffer. Trypsinized cells were incubated in this solution for 30 minutes at 37°C. 500 μM pyocyanin and 5 mM N-acetyl cysteine were added to positive and negative ROS control group cells respectively. Fluorescence intensity was measured from the FL1 line (488 nm) of BD Accuri C6 flow cytometer.

5.1.5 Inductively Coupled PlasmaâMass Spectroscopy (ICP-MS)

Cells in the dishes were briefly rinsed with Ca^{2+}-free phosphate buffered saline and scraped into deionized water containing 1% Triton X-100 (Merck). Total protein concentration in lysates were measured with Bradford assay (Bio-rad). 4 ml, 65% nitric acid and 1 ml, 30% hydrogen peroxide were added to each lysate before a microwave digestion protocol under 45 bar pressure at 180°C, to ensure the solvation of protein-bound ions. Ca^{2+} and Zn^{2+} concentrations measured by Agilent 7700X ICP-MS instrument. R^2 values standard curves were 0.999 for both ions and detection limits were calculated as 14.43 ppb and 0.53 ppb for Ca^{2+} and Zn^{2+}, respectively. Measurements from samples were normalized to protein concentration in each sample to enable comparison.

5.1.6 Intracellular Cation Imaging and Store-Operated Ca^{2+} Entry (SOCE) Experiments

Fluo-8 AM (Santa Cruz, CalciFluor) Ca^{2+} indicator was used along with either fluorescence microscopy or flow cytometry for comparative evaluation of intracellular cations and SOCE. The indicator stock solution was prepared in DMSO and diluted to 5μM in serum-free medium. For flow cytometry experiments, cells were trypsinized,

centrifuged and re-dispersed in loading medium. At the end of the 30-minute dye loading period at room temperature, cells were centrifuged and washed 3 times with fresh serum-free medium. Fluorescence signal was measured by BD Accuri C6 flow cytometer and analyzed using the peak area (FL1-A) parameter of the FL1 (488 nm) line. In order to isolate the Ca^{2+} signal from the non-specific interactions of Fluo-8 with other cations, 5 μM TPEN was added to the loading and washing media. For fluorescence microscopy, loading medium was directly added on the coverslips after washing and loaded for 30 minutes at room temperature. Cells were washed, imaged and the captured images were processed with ImageJ software. Mean fluorescence intensity of each cell area was measured comparatively to background.

Imaging of endoplasmic reticulum (ER) stores was performed by utilizing the compartmentalization of Ca^{2+} probes into ER after prolonged incubation [155]. Cells on coverslips were incubated with loading medium for 2 hours at 37°C, washed and labeled with ER-Tracker blue-white (Thermo fisher). Indicator molecules remaining in the cytosol were removed by selective permeabilization of the plasma membrane using a 0.5% solution of saponin in intracellular buffer containing 125 mM KCl, 25 mM NaCl, 10 mM HEPES, 0.2 mM $CaCl_2$, 0.5 mM EGTA, 0.2 mM $MgCl_2$ and 0.5 mM ATP. After 5 minutes of permeabilization, cells were washed with more intracellular buffer and images were captured.

SOCE experiments were performed by time dependent flow cytometry measurements. Cells were trypsinized, loaded with fluo-8 and re-dispersed in extracellular fluid composed of 125 mM NaCl, 5 mM KCl, 1 mM $MgCl_2$, 1 mM KH_2PO_4, 5.5 mM glucose, 1 mM $CaCl_2$, 20 mM HEPES and 10 mg/ml BSA. During flow cytometry measurements, the runs were paused after 3 minutes and 2 μM thapsigargin was added to the cells before immediately restarting the run. Control runs were performed with DMSO addition and Ca^{2+} free extracellular fluid. Median FL1-A fluorescence was analyzed on time axis using FlowJo software. SOCE was expressed as fold increase in FL1-A intensity after thapsigargin addition.

5.1.7 Statistical Analyses

Mann-Whitney test was used to compare ranks of populations whenever only two populations were present such as Tuj1 western, ROS, ICP-MS and mitochondrial polarization results. When both 50 Hz ELF EMF and an additional treatment were used, the effect was tested with two-way ANOVA. Each individual flow cytometry experiment was tested between sham and 50 Hz ELF EMF groups by comparing the populations with Mann-Whitney test. In order to see the changes that occur to the difference between these groups by treatment with different chemicals, each sham vs 50 Hz flow cytometry experiment was expressed as a resolution metric (R_D) which was calculated according to Eq. 5.1:

$$R_D = \frac{Median_{50Hz} - Median_{Sham}}{rSD_{50Hz} + rSD_{Sham}} \tag{5.1}$$

where rSD corresponds to the robust standard deviation of each sample's fluorescence histogram. R_D of each experiment represents the change in signal intensity between sham and 50 Hz groups independently from dye loading efficiency or instrumental effects enabling comparison between experiments performed at different times. R_D values of at least 3 replica experiments were pooled and the differences were tested using two-way ANOVA. Tests were performed using Graphpad prism and calculated p values were symbolized as n.s, one, two or three asterisks to show $p>0.05$, $p<0.05$, $p<0.01$ and $p<0.001$ respectively.

5.2 Results

5.2.1 50 Hz ELF EMF Exposure Effects on Tuj1 and ROS Levels

Induction of neural markers and ROS are commonly reported effects of 50 Hz ELF EMFs in the literature [109, 115, 116, 156]. In an attempt to confirm these observations, neural marker Tuj1 and intracellular ROS levels of BM-MSCs were probed after 7 days of 50 Hz ELF EMF exposure.

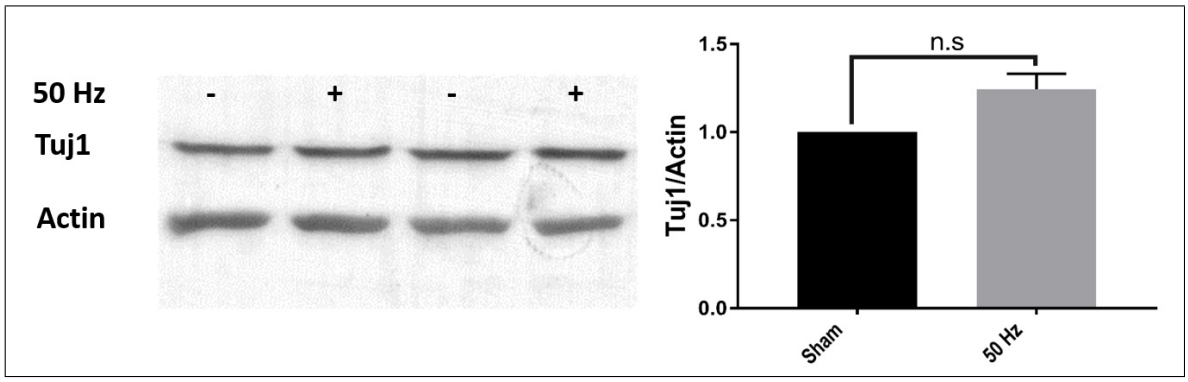

Figure 5.1 Tuj1 levels of sham and 50 Hz ELF EMF exposed BM-MSCs measured by western blot.

Repeated western blot experiments failed to display a visible change in Tuj1 levels and quantification of blots also returned a non-significant result after Mann-Whitney test (Figure 5.1). This may be attributed to the fact that previous studies frequently used qPCR to detect changes in expression of target markers but seldom probed the actual protein levels with western blot or a similar method [96, 115, 137]. This finding indicates that surges in expression of certain markers under ELF EMF exposure could be compensated by post-transcriptional modifications. On the other hand, ROS induction effect reported in the literature was confirmed by these results.

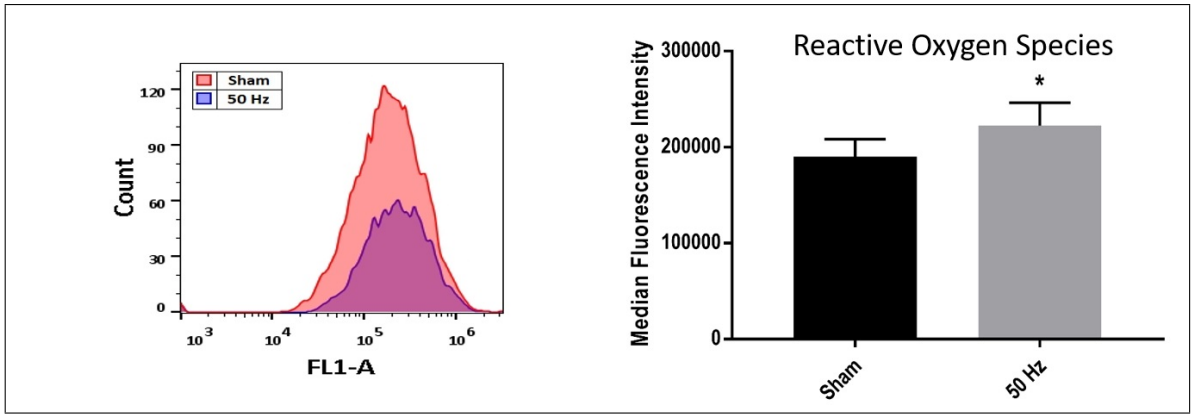

Figure 5.2 Increase in intracellular ROS levels as measured by total ROS assay kit and flow cytometry, along with a sample histogram.

Flow cytometry experiments conducted with a fluorescent total ROS indicator consistently showed an increase between 50 Hz ELF EMF and sham groups, resulting

in a mean R_D value of 0.064 ∓ 0.018 between groups. Figure 5.2 shows the pooled median fluorescence intensity values along with a sample histogram. P value between the groups in pooled data was calculated as 0.027.

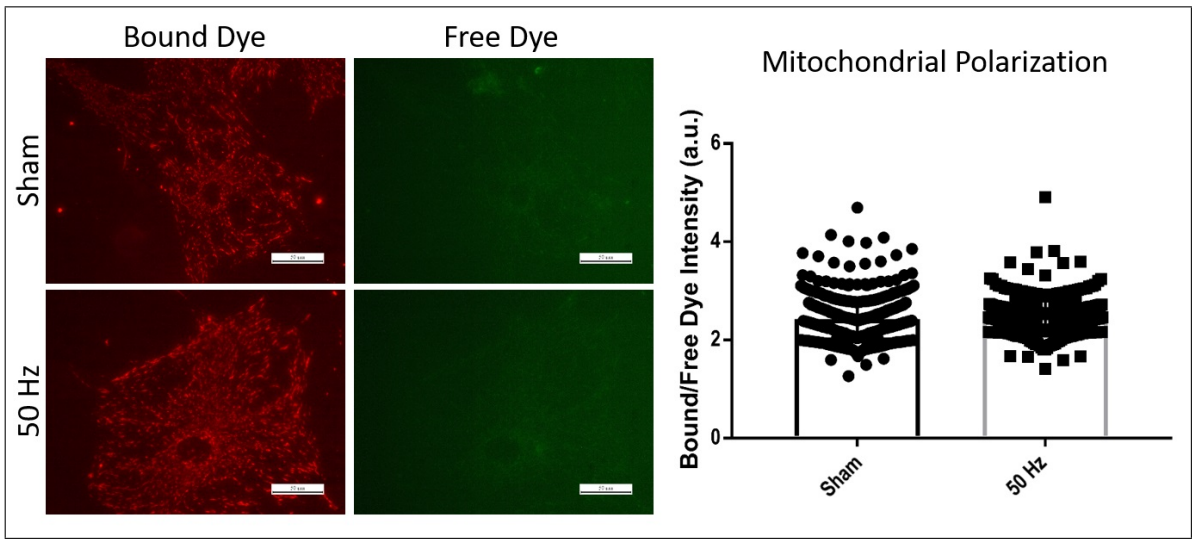

Figure 5.3 Mitochondrial membrane potentials as evaluated by JC-1 staining and sample micrographs.

The lack of information about the source of ELF EMF-induced ROS elevation prompted an investigation into mitochondria, a major source of intracellular ROS. Since polarization of mitochondrial membrane is associated with its metabolic state and ROS generation levels [157], mitochondrial membrane potential was probed using the voltage sensitive dye JC-1. However, as seen in Figure 5.3, no changes were detected in the ratio of bound to free dye molecules, which is a direct function of the membrane voltage. The result implicates that effects on ROS generating or scavenger enzymes such as NADPH oxidase or superoxide dismutase are more likely candidates for the emergence of this effect.

5.2.2 50 Hz ELF EMF-invoked Ca^{2+} Influx is Accompanied by a Zn^{2+} Influx

Previous reports of ELF EMF-evoked Ca^{2+} increase did not correct (by using appropriate chelators) for non-specific binding of Ca^{2+} probes to Zn^{2+} [120], which reveals a possibility for an undiscovered Zn^{2+} influx. Data shows that when this correction is applied by using Zn^{2+} chelator TPEN during intracellular Ca^{2+} labeling, a marked reduction occurs in the difference between sham and 50 Hz ELF EMF groups (Figure 5.4). This was achieved by including the Zn^{2+} chelator TPEN in the dye loading medium to prevent binding of Ca^{2+} indicator Fluo-8 to Zn^{2+} and isolate the Ca^{2+} signal from other metal interactions [158].

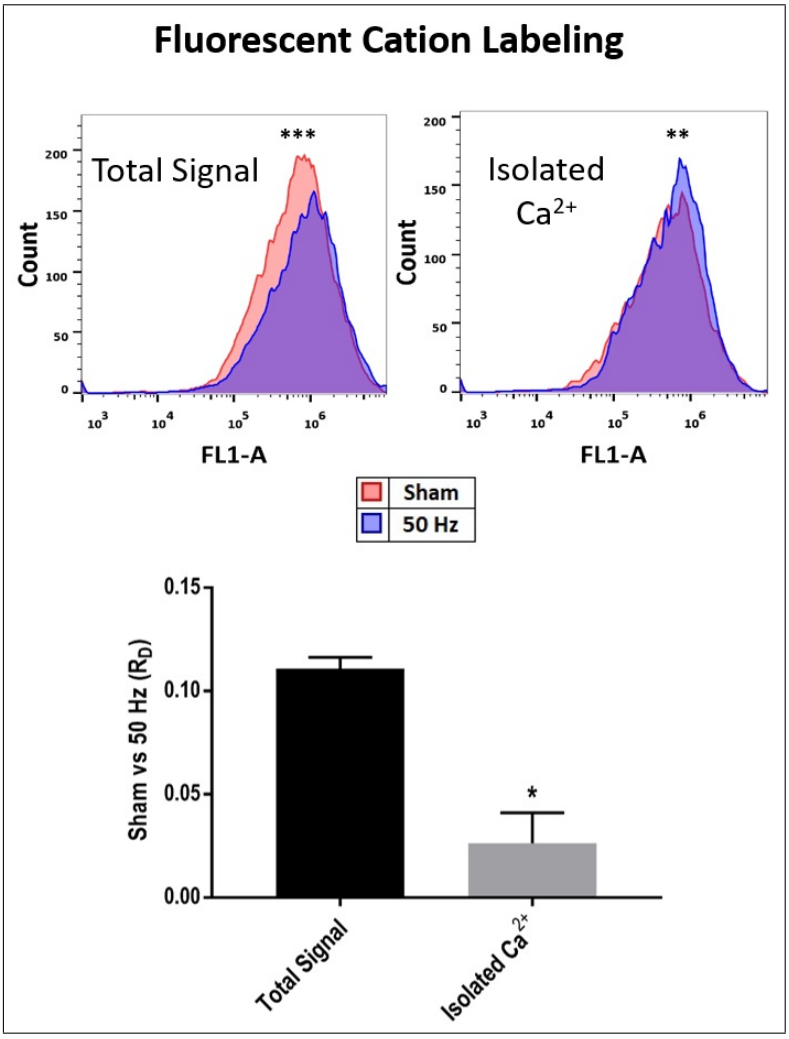

Figure 5.4 Levels of intracellular cations as measured by Fluo-8 staining and TPEN correction for isolating the Ca^{2+} signal from Zn^{2+}. Sample histograms are given at the top.

In uncorrected experiments, 50 Hz ELF EMF groups' median fluorescence intensity showed a 1.309∓0.002-fold increase over sham groups while this difference was reduced to 1.058∓0.043 fold when Ca^{2+} signal was isolated. Calculated R_D values of Zn^{2+} corrected experiments were also significantly lower than uncorrected experiments (p=0.033), indicating that 50 Hz ELF EMF-induced Ca^{2+} intake could be accompanied by a Zn^{2+} influx.

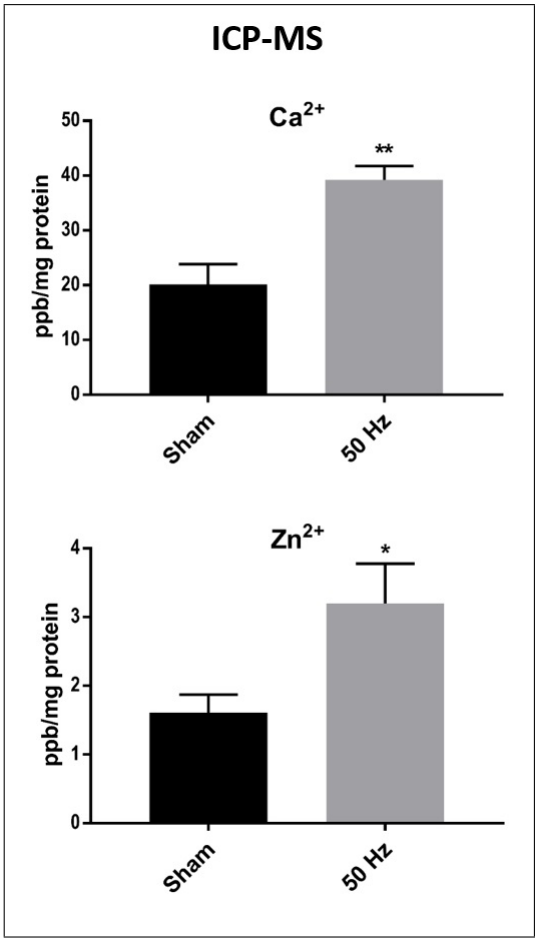

Figure 5.5 Total intracellular concentrations of Ca^{2+} and Zn^{2+} as measured by ICP-MS from total cell lysates.

In order to confirm that the observed phenomenon is an actual Zn^{2+} influx and not a mere increased availability of intracellular Zn^{2+}, absolute concentrations of these cations were measured using ICP-MS. Total intracellular concentrations of both Ca^{2+} and Zn^{2+} showed an almost two-fold increase on average (Figure 5.5). It is important to realize that these measurements were performed on whole cell lysates that were digested under high temperature and pressure in order to solubilize protein-bound ions

and thus represents the entire intracellular ion content as opposed to labeling of free ion populations with indicators. This finding confirms that 50 Hz ELF EMF exposure causes an influx of Zn^{2+} in addition to previously reported Ca^{2+}. Furthermore, this data shows for the first time that 50 Hz ELF EMF-evoked increase in cytosolic Ca^{2+} is the result of an influx and not a release from intracellular stores or a balance shift in cytosolic buffers.

5.2.3 Eliminating TRP channels or intracellular Zn^{2+} prevents ion influx

Identifying the types of channels that facilitate the cation influx is a major milestone for understanding the exact mechanisms by which ELF EMFs interact with cells. In the case of this thesis, the increased permeability of the cells to two different ions suggests the TRP family as a group of non-selective channels as a candidate [159]. However, L-type voltage gated Ca^{2+} channels also show some degree of permeability (8-10% of Ca^{2+} currents) towards Zn^{2+} [160,161]. In an attempt to reveal the involvement of specific channels in the cation influx, cells were treated with a blocker panel during the period of incubation under 50 Hz ELF EMF exposure. 2-APB is able to block currents through most of the TRPC subfamily [162] and also some TRPM subtypes so it is generally accepted as a broad range inhibitor of the TRP family [163–165]. Nifedipine was used as a blocker of L-type Ca^{2+} channels [166]. Gabapentin and ethosuximide were included in the panel to selectively inhibit high-threshold channel types and low-voltage activated T-type Ca^{2+} channels respectively [167, 168]. Earlier results have shown that NMDA receptors are largely responsible from 50 Hz ELF EMF effects on neural stem cells. Since there are reports of NMDA receptor involvement in Zn^{2+} permeation in the literature [161], memantine was also included in this panel as an NMDA receptor inhibitor [169].

When cells were loaded with Fluo-8 and analyzed with fluorescence microscopy, the signal increase with 50 Hz ELF EMF exposure could be detected, as previously observed by flow cytometry experiments. Memantine, nifedipine or gabapentin could not eliminate this effect as presented in Figure 5.6. Conversely, in the groups treated

with ethosuximide and 2-APB, 50 Hz ELF EMF-induced cation intake was neutralized as evidenced by cell populations displaying statistically similar fluorescence intensities. The finding indicates involvement of low-threshold currents of T-type Ca^{2+} channels or the TRP family in the cation influx. However, this method was not able to isolate one of them as the main pathway of cation entry.

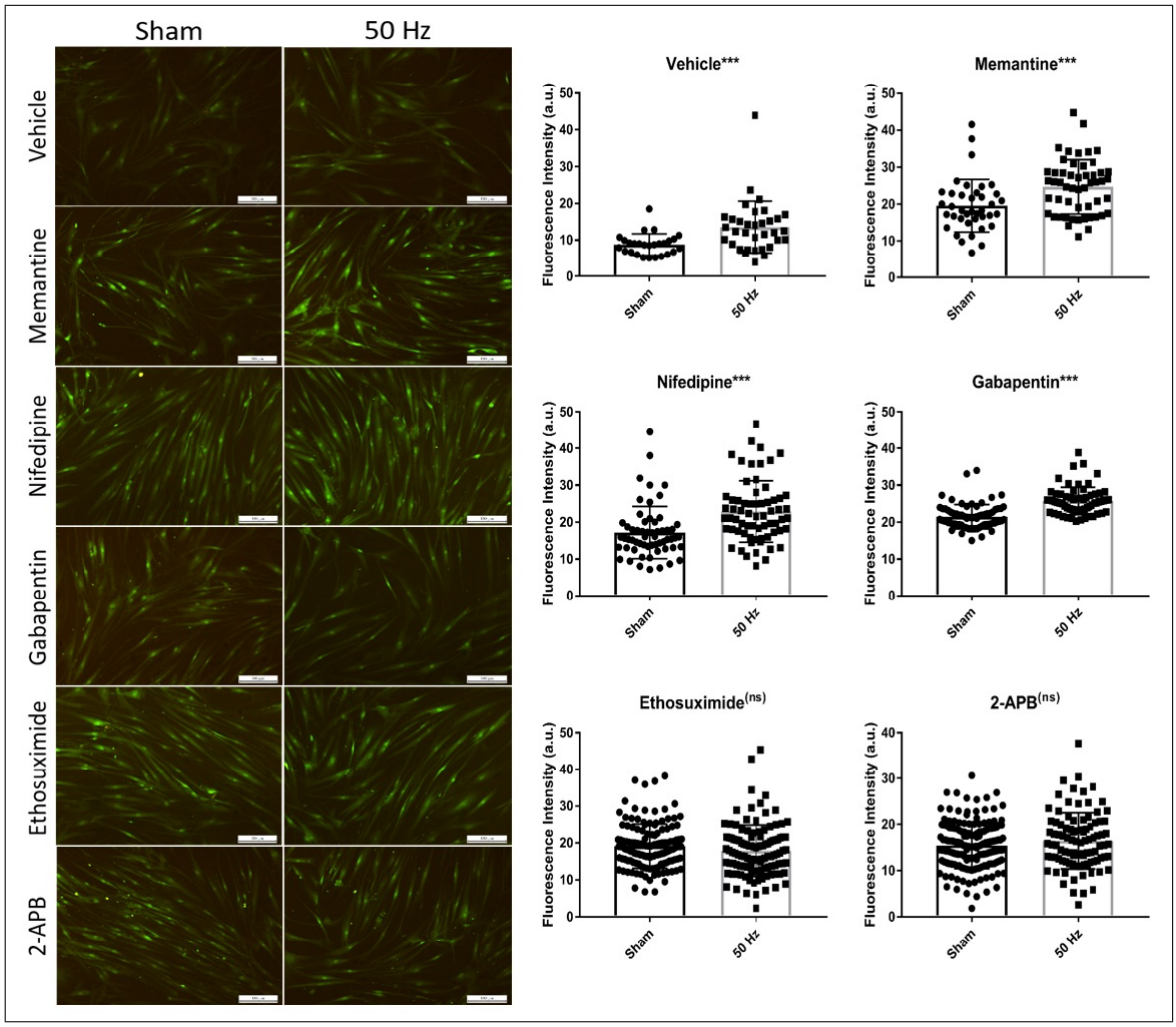

Figure 5.6 Fluo-8 staining applied to cells treated with the blockers, TPEN and Zn^{2+} and measured by fluorescence microscopy. Results are given alongside sample fluorescence micrographs.

In order to further scrutinize this finding and discern between the roles of T-type Ca^{2+} channels and TRP family, the phenomenon was analyzed with a more sensitive method. Since 50 Hz ELF EMF-induced influx of Zn^{2+} was previously identified, additional groups were included to test their further involvement in the cation intake. In order to assess the role of intracellular Zn^{2+}, a non-cytotoxic concentration of TPEN

[170] was applied to BM-MSCs during differentiation and in a separate group, serum-free medium was supplemented with 5 μM Zn^{2+} in addition to the 1.5 μM that was already in the formulation [171].

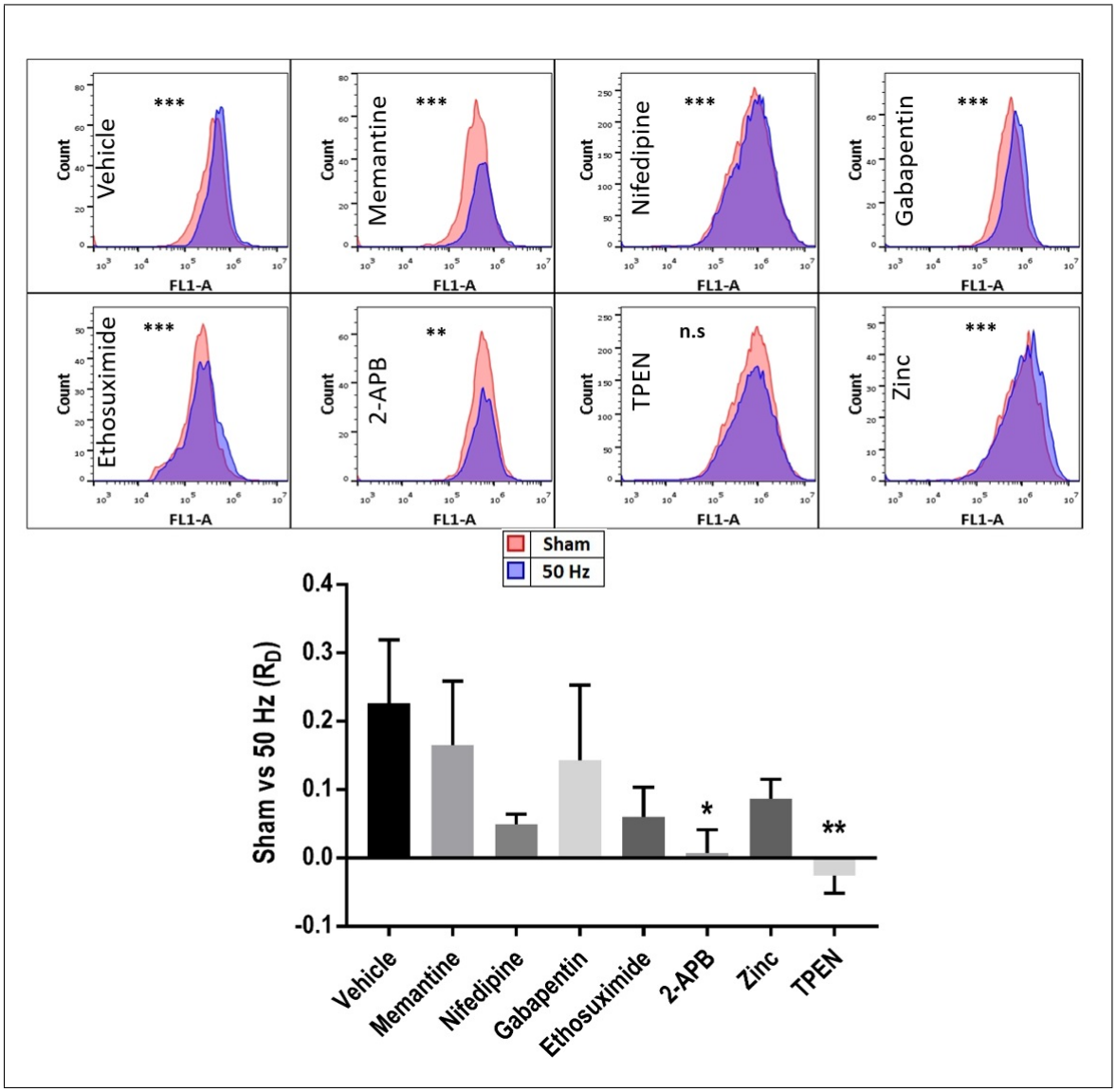

Figure 5.7 Fluo-8 staining applied to cells treated with the blockers, TPEN and Zn^{2+} and measured by flow cytometry shown alongside sample histograms.

Owing to the high sensitivity and statistical power of flow cytometry, a much more definitive answer was revealed by these experiments. First of all, populations with statistically identical fluorescence signal could only be achieved in the TPEN-treated group and none of the blockers could completely eliminate the cation intake (Figure 5.7). When data from repeated experiments were being evaluated, each pair of Sham

vs 50 Hz histograms were expressed as R_D values, which represent the amount of signal increase in 50 Hz groups while accounting for the spread of the populations for each sample [172]. When repeated measures of R_D were pooled the difference created by 50 Hz ELF EMF exposure could be compared between the groups. The R_D values graphed in Figure 5.7 were tested with two-way ANOVA and post-hoc analysis was performed to compare each treatment with vehicle. The result shows that, all treatments except 2-APB and TPEN failed to reduce the difference caused by 50 HZ ELF EMF exposure to statistically discernible levels. The fact that TPEN treatment results in statistically identical population distributions concludes that intracellular Zn^{2+} is essential for 50 Hz ELF EMF-induced cation intake. On the other hand, 2-APB treatment causes a marked decrease but not eliminate the influx, implying multiple routes of entry. The effect of ethosuximide observed with fluorescence microscopy was not confirmed by the flow cytometry results and this was attributed to limited sensitivity and sample size of the method. Other voltage gated Ca^{2+} channels and NMDA receptors were confirmed to not play a part in the effect. Moreover, additional Zn^{2+} in the extracellular space did not amplify the effect.

Regarding the discrepancy between these findings and previous results with NMDA receptors in the earlier results on hNPCs, the disagreement could be explained by the expression differences of ion channel types. This prediction was verified by assaying channel subunits with a western blot seen in Figure 5.8. The voltage gated Ca^{2+} channel subunit Cacna2d1 could be detected in both sham and 50 Hz groups whereas NMDA receptor subunit NR2A was below detection limits of the technique. This finding exhibits the importance of variations in model, underlining the reason of countless contradicting results in the literature and the difficulty of performing meta-analyses with the available data.

In an attempt to eliminate the probability of SOCE and Orai channel involvement, SOCE was tested in sham and 50 Hz ELF EMF exposure groups. Besides the TRP family, 2-APB is also a known inhibitor of SOCE through uncertain mechanisms [173] and it's necessary to verify that the effects observed with 2-APB are due to interactions with TRP family, not disruptions of SOCE. Thapsigargin-induced Ca^{2+}

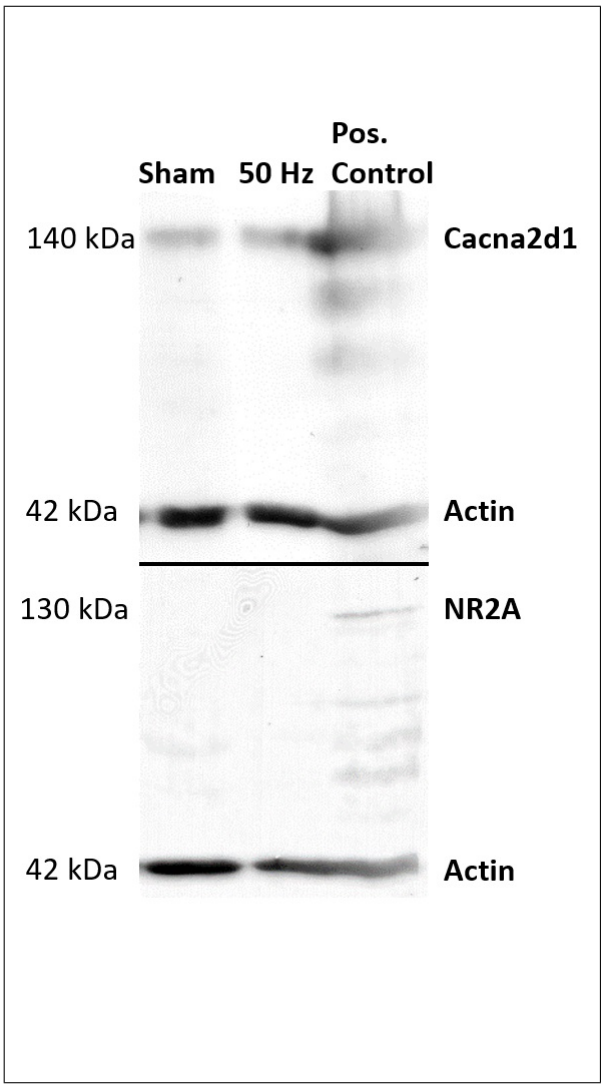

Figure 5.8 Western blot detection of voltage gated Ca^{2+} channel subunit Cacna2d1 and NMDA receptor subunit NR2A.

intake was measured in both groups using flow cytometry. The signal increase upon Ca^{2+} mobilization was around 1.8-fold for both groups and results were statistically identical ($p>0.900$) as reported in Figure 5.9.

In the final part of the thesis, it was tested to see whether 50 Hz ELF EMF exposure has any effects on ER Ca^{2+} stores. Utilizing the compartmentalization of Fluo-8 following prolonged incubation, signals from the ER stores of Ca^{2+} were shown to slightly increase ($p=0.028$) after 50 Hz ELF EMF exposure in Figure 5.10. This finding serves as a verification of the ICP-MS results where the cation levels show large increases that cannot be explained by solely to the changes in relatively low cytosolic

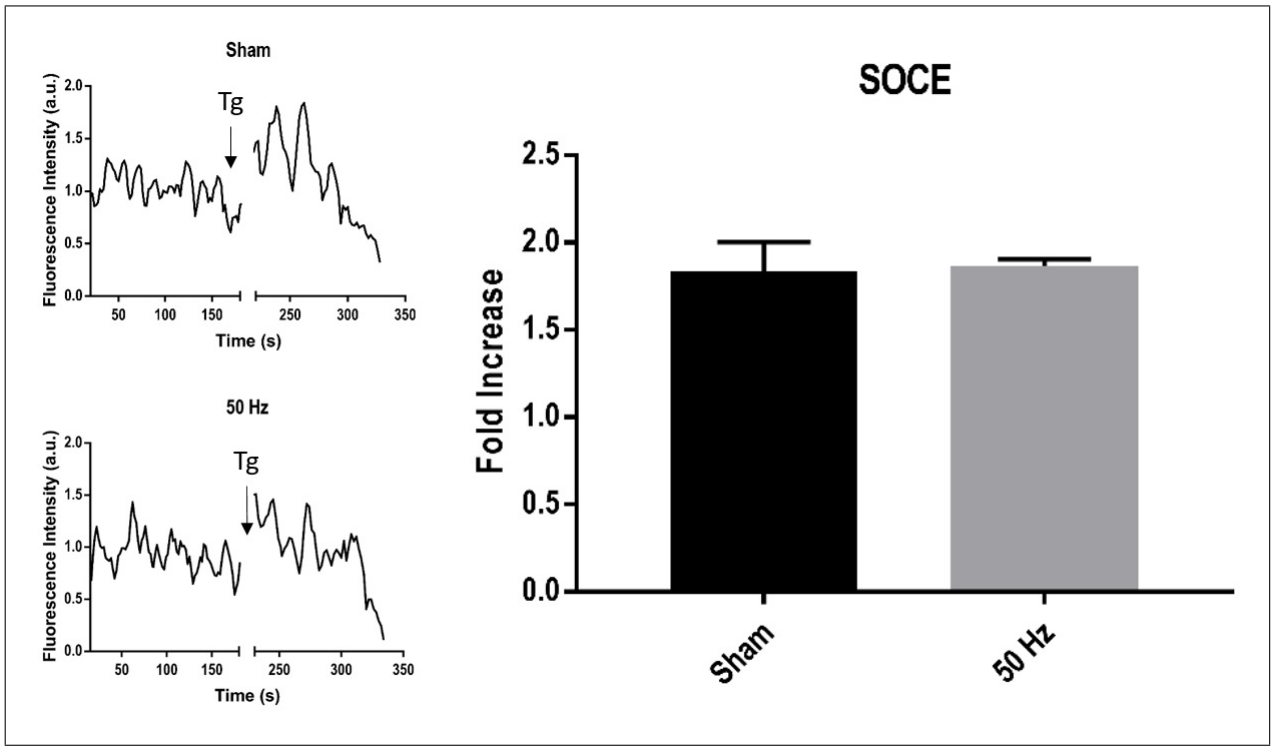

Figure 5.9 Thapsigargin induced Ca^{2+} intake results measured by flow cytometry given with sample time-dependent median fluorescence intensity graphs.

concentrations. This means that the Ca^{2+} uptake occurring under the effect of 50 Hz ELF EMF is large enough to trigger ER regulation and affect the store levels. Unfortunately, it was not possible to utilize the high volume data advantage of flow cytometry in these experiments. Since the imaging is performed while the plasma membrane is perforated, the shear stress of flow caused the cells to rapidly die and shed debris during the measurements, preventing data acquisition.

5.3 Discussion

Efforts towards identifying exact interaction mechanisms of ELF EMFs with biological systems are hindered by contradicting data gathered from different models. However, one commonly agreed upon effect seems to be an increase of intracellular Ca^{2+} across the literature, which makes it an ideal starting point for a mechanistic

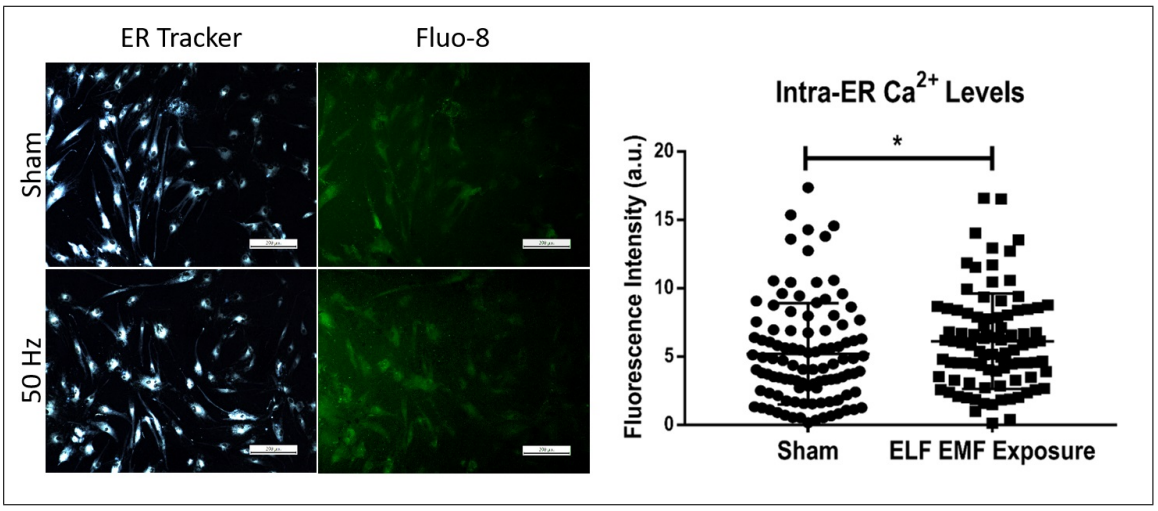

Figure 5.10 Cation levels of ER pools measured by compartmentalization of Fluo-8 and fluorescence microscopy.

investigation. Obtained results do verify an influx of extracellular Ca^{2+}, but with the additional discovery of concomitant Zn^{2+} intake. This finding suggests the involvement of non-selective ion channels as a way to conduct both cations. Results show that the TRP channel family, which include Zn^{2+} permeable members [174], not voltage gated channels have a significant role in the cation intake. The members of this family are highly diverse in gating kinetics and function with new data still rapidly becoming available in the literature [175–177]. In this sense, discovering 2-APB dependence of ELF EMF-induced cation intake only serves as a preliminary finding and not in any way conclude that one or multiple member/s of this family are directly activated by ELF EMF exposure. It is also important to realize that, after the first TPEN correction to isolate Ca^{2+} signals in flow cytometry, all other experiments were run without this correction, thus represents and referred to as total cation intake. The evidence in this thesis does not rule out the possibility that Zn^{2+} and Ca^{2+} intake can occur sequentially or through separate gateways that are activated as part of an ELF EMF-triggered cascade. Other transporters selective for Zn^{2+} [178] can also be involved. However, it can be concluded that, whether through a single channel or a cascade, the entire series of events leading to ELF EMF-induced cation intake is absolutely dependent upon the presence of intracellular Zn^{2+}. For future studies, investigation of Zn^{2+}-modulated pathways and channels, Zn^{2+}-ROS interplay along with knock-in/out studies with specific TRP members is recommended.

6. CONCLUSION

In summary, the part of this thesis regarding mechanotransduction concludes that when evaluating SH-SY5Y differentiation in the context of substrate stiffness, morphological parameters should not be taken at face value. When electrophysiological and biochemical elements are involved, the neuronal behavior is enhanced on soft substrates, conflicting with the decreased neuritogenesis. Electrophysiological responsiveness of SH-SY5Y cells is found to be directly dependent on the substrate elasticity. Moreover, when the substrate stiffness becomes small enough to mimic neural tissue ECM, abundance of neural marker TUJ 1 is significantly elevated. These results reveal useful information about SH-SY5Y model and mechano-regulation aspect of neuronal differentiation.

The findings about ELF EMF exposure show that it amplifies neuronal differentiation of hNPCs in an NMDA receptor dependent manner. Other previously reported effects such as elevation of c-fos levels, intracellular Ca^{2+} and elongated neurites are also demonstrated to be facilitated by NMDA receptor activation. These findings allow us to postulate that effects of ELF EMF on neural differentiation is initiated by its effects on activation mechanisms of NMDA receptors. In essence, this work identifies NMDA receptors as a strong candidate for future studies which pursues interaction mechanisms of ELF MF with neural tissues.

Concerning the BM-MSC model of neural differentiation, findings show that 50 Hz ELF EMF-induced upregulation of neural markers do not always make it all the way to translation and ROS, generated by ELF EMF exposure is unlikely to be caused by effects on mitochondrial state. Most importantly, the data demonstrate a previously unknown Zn^{2+} influx accompanying 50 Hz ELF EMF-induced Ca^{2+} intake and present evidence towards involvement of TRP channel family in the total cation intake. The report presents Zn^{2+} and the TRP family as new and strong candidates for mechanistic investigations into ELF EMF interactions with biological systems.

All in all, this thesis reveals novel mechanistic clues about the interactions of biophysical factors with neural differentiation pathways in three distinct biological models. These will not only benefit future researchers using these models, they will also contribute to discovery and utilizations of intracellular molecular machinery that sense and respond to biophysical stimuli. The understanding of which will undoubtedly advance efforts towards modeling and treating neurodegenerative diseases.

REFERENCES

1. "What is biophysics? | the biophysical society," 0. [Online; accessed 2020-12-30].

2. Prendergast, P. J., R. Huiskes, and K. Soballe, "Biophysical stimuli on cells during tissue differentiation at implant interfaces," *Journal of Biomechanics*, 1997.

3. Okamoto, K., A. Germond, H. Fujita, C. Furusawa, Y. Okada, and T. M. Watanabe, "Single cell analysis reveals a biophysical aspect of collective cell-state transition in embryonic stem cell differentiation," *Scientific Reports*, 2018.

4. Govey, P. M., A. E. Loiselle, and H. J. Donahue, "Biophysical regulation of stem cell differentiation," *Current Osteoporosis Reports*, 2013.

5. Gurkan, U. A., and O. Akkus, "The mechanical environment of bone marrow: A review," *Annals of Biomedical Engineering*, 2008.

6. Shaw, N. E., "Studies on intramedullary pressure and blood flow in bone," *American Heart Journal*, 1964.

7. Yamamoto, K., T. Sokabe, T. Watabe, K. Miyazono, J. K. Yamashita, S. Obi, N. Ohura, A. Matsushita, A. Kamiya, and J. Ando, "Fluid shear stress induces differentiation of flk-1-positive embryonic stem cells into vascular endothelial cells in vitro," *American Journal of Physiology - Heart and Circulatory Physiology*, 2005.

8. Masumura, T., K. Yamamoto, N. Shimizu, S. Obi, and J. Ando, "Shear stress increases expression of the arterial endothelial marker ephrinb2 in murine es cells via the vegf-notch signaling pathways," *Arteriosclerosis, Thrombosis, and Vascular Biology*, 2009.

9. Illi, B., S. Nanni, A. Scopece, A. Farsetti, P. Biglioli, M. C. Capogrossi, and C. Gaetano, "Shear stress-mediated chromatin remodeling provides molecular basis for flow-dependent regulation of gene expression," *Circulation Research*, 2003.

10. Henrionnet, C., Y. Wang, E. Roeder, N. Gambier, L. Galois, D. Mainard, D. Bensoussan, P. Gillet, and A. Pinzano, "Effect of dynamic loading on mscs chondrogenic differentiation in 3-d alginate culture," *Bio-Medical Materials and Engineering*, 2012.

11. Cao, W., W. Lin, H. Cai, Y. Chen, Y. Man, J. Liang, Q. Wang, Y. Sun, Y. Fan, and X. Zhang, "Dynamic mechanical loading facilitated chondrogenic differentiation of rabbit bmscs in collagen scaffolds," *Regenerative Biomaterials*, 2019.

12. Fahy, N., M. Alini, and M. J. Stoddart, "Mechanical stimulation of mesenchymal stem cells: Implications for cartilage tissue engineering," *Journal of Orthopaedic Research*, 2018.

13. Kim, H. K., J. H. Kim, A. A. Abbas, D. O. Kim, S. J. Park, J. Y. Chung, E. K. Song, and T. R. Yoon, "Red light of 647 nm enhances osteogenic differentiation in mesenchymal stem cells," *Lasers in Medical Science*, 2009.

14. Lim, J. Y., J. C. Hansen, C. A. Siedlecki, J. Runt, and H. J. Donahue, "Human foetal osteoblastic cell response to polymer-demixed nanotopographic interfaces," *Journal of the Royal Society Interface*, 2005.

15. Lim, J. Y., A. E. Loiselle, J. S. Lee, Y. Zhang, J. D. Salvi, and H. J. Donahue, "Optimizing the osteogenic potential of adult stem cells for skeletal regeneration," *Journal of Orthopaedic Research*, 2011.

16. Lv, H., L. Li, M. Sun, Y. Zhang, L. Chen, Y. Rong, and Y. Li, "Mechanism of regulation of stem cell differentiation by matrix stiffness," *Stem Cell Research and Therapy*, 2015.

17. Leone, L., M. V. Podda, and C. Grassi, "Impact of electromagnetic fields on stem cells: Common mechanisms at the crossroad between adult neurogenesis and osteogenesis," *Frontiers in Cellular Neuroscience*, 2015.

18. Salvador, R., P. C. Miranda, Y. Roth, and A. Zangen, "High-permeability core coils for transcranial magnetic stimulation of deep brain regions," pp. 6652–6655, 2007.

19. Edwards, R. G., "Ivf and the history of stem cells," *Nature*, 2001.

20. Stadtfeld, M., and K. Hochedlinger, "Induced pluripotency: History, mechanisms, and applications," *Genes and Development*, 2010.

21. Bhartiya, D., "Are mesenchymal cells indeed pluripotent stem cells or just stromal cells? oct-4 and vsels biology has led to better understanding," *Stem Cells International*, 2013.

22. Bianco, P., P. G. Robey, and P. J. Simmons, "Mesenchymal stem cells: Revisiting history, concepts, and assays," *Cell Stem Cell*, 2008.

23. Ming, G. L., and H. Song, "Adult neurogenesis in the mammalian central nervous system," *Annu Rev Neurosci*, Vol. 28, pp. 223–250, 2005.

24. Paton, J. A., and F. N. Nottebohm, "Neurons generated in the adult brain are recruited into functional circuits.," *Science (New York, N.Y.)*, Vol. 225, no. 4666, pp. 1046–8, 1984.

25. Reynolds BA, W. S., "Generation of neurons and astrocytes from isolated cells of the adult mammalian central nervous system," *Science*, Vol. 255, no. 5052, pp. 1707–1710, 1992.

26. Kuhn, H. G., H. Dickinson-Anson, and F. H. Gage, "Neurogenesis in the dentate gyrus of the adult rat: age-related decrease of neuronal progenitor proliferation," *J Neurosci*, Vol. 16, no. 6, pp. 2027–2033, 1996.

27. Eriksson, P. S., E. Perfilieva, T. Bjork-Eriksson, A. M. Alborn, C. Nordborg, D. A. Peterson, and F. H. Gage, "Neurogenesis in the adult human hippocampus.," *Nature Medicine*, Vol. 4, no. 11, pp. 1313–7, 1998.

28. Gage, F. H., "Mammalian neural stem cells," *Science*, Vol. 287, no. 5457, pp. 1433–1438, 2000.

29. Hollands, C., N. Bartolotti, and O. Lazarov, "Alzheimer's disease and hippocampal adult neurogenesis; exploring shared mechanisms," *Frontiers in Neuroscience*, Vol. 10, 2016.

30. Marxreiter, F., M. Regensburger, and J. Winkler, "Adult neurogenesis in parkinson's disease," *Cellular and Molecular Life Sciences*, Vol. 70, no. 3, pp. 459–473, 2013.

31. Elvira, G., I. Garcia, J. Gallo, M. Benito, P. Montesinos, E. Holgado-Martin, A. Ayuso-Sacido, S. Penades, M. Desco, A. Silva, and J. A. Garcia-Sanz, "Detection of mouse endogenous type b astrocytes migrating towards brain lesions," *Stem Cell Research*, Vol. 14, no. 1, pp. 114–129, 2015.

32. Doetsch, F., I. Caille, D. A. Lim, J. M. Garcia-Verdugo, and A. Alvarez-Buylla, "Subventricular zone astrocytes are neural stem cells in the adult mammalian brain," *Cell*, Vol. 97, no. 6, pp. 703–716, 1999.

33. Laywell, E. D., P. Rakic, V. G. Kukekov, E. C. Holland, and D. A. Steindler, "Identification of a multipotent astrocytic stem cell in the immature and adult mouse brain," *Proceedings of the National Academy of Sciences*, Vol. 97, no. 25, pp. 13883–13888, 2000.

34. Azari, H., and B. A. Reynolds, "In vitro models for neurogenesis," *Cold Spring Harbor Perspectives in Biology*, 2016.

35. Bond, A. M., G. L. Ming, and H. Song, "Adult mammalian neural stem cells and neurogenesis: Five decades later," *Cell Stem Cell*, 2015.

36. Shi, Y., P. Kirwan, and F. J. Livesey, "Directed differentiation of human pluripotent stem cells to cerebral cortex neurons and neural networks," *Nature Protocols*, 2012.

37. Cho, K. J., K. A. Trzaska, S. J. Greco, J. McArdle, F. S. Wang, J.-H. Ye, and P. Rameshwar, "Neurons derived from human mesenchymal stem cells show synaptic transmission and can be induced to produce the neurotransmitter substance p by interleukin-1alpha," *Stem Cells*, 2005.

38. Greco, S. J., C. Zhou, J. H. Ye, and P. Rameshwar, "An interdisciplinary approach and characterization of neuronal cells transdifferentiated from human mesenchymal stem cells," *Stem Cells and Development*, 2007.

39. Montzka, K., N. Lassonczyk, B. Tschoke, S. Neuss, T. Fuhrmann, R. Franzen, R. Smeets, G. A. Brook, and M. Woltje, "Neural differentiation potential of human bone marrow-derived mesenchymal stromal cells: Misleading marker gene expression," *BMC Neuroscience*, 2009.

40. Scuteri, A., M. Miloso, D. Foudah, M. Orciani, G. Cavaletti, and G. Tredici, "Mesenchymal stem cells neuronal differentiation ability: A real perspective for nervous system repair?," *Current Stem Cell Research Therapy*, 2011.

41. Shahbazi, A., M. Safa, F. Alikarami, S. Kargozar, M. H. Asadi, M. T. Joghataei, and M. Soleimani, "Rapid induction of neural differentiation in human umbilical cord matrix mesenchymal stem cells by camp-elevating agents.," *International Journal of Molecular and Cellular Medicine*, Vol. 5, no. 3, pp. 167–177, 2016.

42. Thompson, R., C. Casali, and C. Chan, "Forskolin and ibmx induce neural transdifferentiation of mscs through downregulation of the nrsf," *Scientific Reports*, 2019.

43. Edsjo, A., L. Holmquist, and S. Pahlman, "Neuroblastoma as an experimental model for neuronal differentiation and hypoxia-induced tumor cell dedifferentiation," *Seminars in Cancer Biology*, Vol. 17, no. 3, pp. 248–256, 2007.

44. Clagett-Dame, M., E. M. McNeill, and P. D. Muley, "Role of all-trans retinoic acid in neurite outgrowth and axonal elongation," *Journal of Neurobiology*, Vol. 66, no. 7, pp. 739–756, 2006.

45. Dow, R., J. Hendley, A. Pirkmaier, E. A. Musgrove, and D. Germain, "Retinoic acid-mediated growth arrest requires ubiquitylation and degradation of the f-box protein skp2," *Journal of Biological Chemistry*, 2001.

46. Cuende, J., S. Moreno, J. P. Bolanos, and A. Almeida, "Retinoic acid downregulates rae1 leading to apc(cdh1) activation and neuroblastoma sh-sy5y differentiation.," *Oncogene*, Vol. 27, no. 23, 2008.

47. Halitzchi, F., L. Jianu, and B. Amuzescu, "Electrophysiology and pharmacology study of a human neuroblastoma cell line," *Romanian Reports in Physics*, Vol. 67, no. 2, pp. 439–451, 2015.

48. Ross, R. A., B. A. Spengler, and J. L. Biedler, "Coordinate morphological and biochemical interconversion of human neuroblastoma cells," *Journal of the National Cancer Institute*, 1983.

49. Xicoy, H., B. Wieringa, and G. J. M. Martens, "The sh-sy5y cell line in parkinson's disease research: a systematic review.," *Molecular Neurodegeneration*, Vol. 12, no. 1, p. 10, 2017.

50. Dwane, S., E. Durack, and P. A. Kiely, "Optimising parameters for the differentiation of sh-sy5y cells to study cell adhesion and cell migration.," *BMC Research Notes*, Vol. 6, no. 1, p. 366, 2013.

51. Kovalevich, J., and D. Langford, "Considerations for the use of sh-sy5y neuroblastoma cells in neurobiology," in *Methods in Molecular Biology (Clifton, N.J.)*, pp. 9–21, 2013.

52. Michael, K. E., D. W. Dumbauld, K. L. Burns, S. K. Hanks, and A. J. Garcia, "Focal adhesion kinase modulates cell adhesion strengthening via integrin activation," *Molecular Biology of the Cell*, 2009.

53. Zhao, X., and J. L. Guan, "Focal adhesion kinase and its signaling pathways in cell migration and angiogenesis," *Advanced Drug Delivery Reviews*, 2011.

54. Encinas, M., M. Iglesias, Y. Liu, H. Wang, A. Muhaisen, V. Cena, C. Gallego, and J. X. Comella, "Sequential treatment of sh-sy5y cells with retinoic acid and brain-derived neurotrophic factor gives rise to fully differentiated, neurotrophic factor-dependent, human neuron-like cells," *Journal of Neurochemistry*, Vol. 75, pp. 991–1003, 2000.

55. Forsythe, I. D., D. G. Lambert, S. R. Nahorski, and P. Linsdell, "Elevation of cytosolic calcium by cholinoceptor agonists in sh-sy5y human neuroblastoma cells: estimation of the contribution of voltage-dependent currents," *British Journal of Pharmacology*, Vol. 107, no. 1, pp. 207–214, 1992.

56. Tosetti, P., V. Taglietti, and M. Toselli, "Functional changes in potassium conductances of the human neuroblastoma cell line sh-sy5y during in vitro differentiation.," *Journal of Neurophysiology*, Vol. 79, no. 2, pp. 648–658, 1998.

57. Santillo, S., A. Schiano Moriello, and V. Di Maio, "Electrophysiological variability in the sh-sy5y cellular line," *General Physiology and Biophysics*, Vol. 33, no. 1, pp. 121–129, 2014.

58. Toselli, M., P. Tosetti, and V. Taglietti, "Functional changes in sodium conductances in the human neuroblastoma cell line sh-sy5y during in vitro differentiation.," *Journal of Neurophysiology*, Vol. 76, no. 6, pp. 3920–7, 1996.

59. Hahn, M., T. Glass, and J. Koke, "Extracellular matrix effects on a neuroblastoma cell line," *Cytobios*, Vol. 102, no. 399, pp. 7–19, 2000.

60. Kruger, T. M., K. J. Bell, T. I. Lansakara, V. A. Tivanski, J. A. Doorn, and L. L. Stevens, "Reduced extracellular matrix stiffness prompts sh-sy5y cell softening and actin turnover to selectively increase ab(1-42) endocytosis," *ACS Chemical Neuroscience*, 2019.

61. Kruger, T. M., K. J. Bell, T. I. Lansakara, V. A. Tivanski, J. A. Doorn, and L. L. Stevens, "A soft mechanical phenotype of sh-sy5y neuroblastoma and primary human neurons is resilient to oligomeric ab(1-42) injury," *ACS Chemical Neuroscience*, 2020.

62. Nam, K.-h., N. Jamilpour, E. Mfoumou, F.-y. Wang, D. D. Zhang, and P. K. Wong, "Probing mechanoregulation of neuronal differentiation by plasma lithography patterned elastomeric substrates.," *Scientific Reports*, Vol. 4, p. 6965, 2014.

63. Lam, W. A., L. Cao, V. Umesh, A. J. Keung, S. Sen, and S. Kumar, "Extracellular matrix rigidity modulates neuroblastoma cell differentiation and n-myc expression.," *Molecular Cancer*, Vol. 9, p. 35, 2010.

64. Goldie, B. J., M. M. Barnett, and M. J. Cairns, "Bdnf and the maturation of posttranscriptional regulatory networks in human sh-sy5y neuroblast differentiation," *Frontiers in Cellular Neuroscience*, 2014.

65. Baraniak, P. R., and T. C. McDevitt, "Stem cell paracrine actions and tissue regeneration," *Regenerative Medicine*, 2010.

66. Discher, D. E., P. Janmey, and Y.-L. Wang, "Tissue cells feel and respond to the stiffness of their substrate.," *Science (New York, N.Y.)*, Vol. 310, no. 5751, pp. 1139–43, 2005.

67. Engler, A. J., S. Sen, H. L. Sweeney, and D. E. Discher, "Matrix elasticity directs stem cell lineage specification," *Cell*, Vol. 126, no. 4, pp. 677–689, 2006.

68. Oliver, W. C., and G. M. Pharr, "Measurement of hardness and elastic modulus by instrumented indentation: Advances in understanding and refinements to methodology," *Journal of Materials Research*, 2004.

69. Mohammed, D., M. Versaevel, C. Bruyere, L. Alaimo, M. Luciano, E. Vercruysse, A. Proces, and S. Gabriele, "Innovative tools for mechanobiology: Unraveling outside-in and inside-out mechanotransduction," *Frontiers in Bioengineering and Biotechnology*, 2019.

70. Narayanan, K., V. Y. Lim, J. Shen, Z. W. Tan, D. Rajendran, S. C. Luo, S. Gao, A. C. Wan, and J. Y. Ying, "Extracellular matrix-mediated differentiation of human embryonic stem cells: Differentiation to insulin-secreting beta cells," *Tissue Engineering - Part A*, 2014.

71. Wang, T., J. H. Lai, L. H. Han, X. Tong, and F. Yang, "Chondrogenic differentiation of adipose-derived stromal cells in combinatorial hydrogels containing cartilage matrix proteins with decoupled mechanical stiffness," *Tissue Engineering - Part A*, 2014.

72. Wang, L., and R. L. Carrier, "Biomimetic topography : Bioinspired cell culture substrates and scaffolds," *Advances in Biomimetics*, pp. 453–472, 2011.

73. Zhang, Q.-Y., Y.-Y. Zhang, J. Xie, C.-X. Li, W.-Y. Chen, B.-L. Liu, X.-a. Wu, S.-N. Li, B. Huo, L.-H. Jiang, and H.-C. Zhao, "Stiff substrates enhance cultured neuronal network activity," *Scientific Reports*, Vol. 4, p. 6215, 2014.

74. Georges, P. C., W. J. Miller, D. F. Meaney, E. S. Sawyer, and P. a. Janmey, "Matrices with compliance comparable to that of brain tissue select neuronal over glial growth in mixed cortical cultures.," *Biophysical Journal*, Vol. 90, no. 8, pp. 3012–3018, 2006.

75. Blaschke, S., S. U. Vay, N. Pallast, M. Rabenstein, J. A. Abraham, C. Linnartz, M. Hoffmann, N. Hersch, R. Merkel, B. Hoffmann, G. R. Fink, and M. A. Rueger, "Substrate

elasticity induces quiescence and promotes neurogenesis of primary neural stem cell-sâa biophysical in vitro model of the physiological cerebral milieu," *Journal of Tissue Engineering and Regenerative Medicine*, 2019.

76. Thompson, A. J., E. K. Pillai, I. B. Dimov, S. K. Foster, C. E. Holt, and K. Franze, "Rapid changes in tissue mechanics regulate cell behaviour in the developing embryonic brain," *eLife*, 2019.

77. Koser, D. E., A. J. Thompson, S. K. Foster, A. Dwivedy, E. K. Pillai, G. K. Sheridan, H. Svoboda, M. Viana, L. D. F. Costa, J. Guck, C. E. Holt, and K. Franze, "Mechanosensing is critical for axon growth in the developing brain," *Nature Neuroscience*, 2016.

78. Tate, M. C., A. J. GarcÃa, B. G. Keselowsky, M. A. Schumm, D. R. Archer, and M. C. Laplaca, "Specific b 1 integrins mediate adhesion, migration, and differentiation of neural progenitors derived from the embryonic striatum," *Molecular and Cellular Neuroscience*, 2004.

79. Mariscalco, M. M., "Integrins and cell adhesion molecules," in *Fetal and Neonatal Physiology: Third Edition*, 2003.

80. Ingber, D. E., "From cellular mechanotransduction to biologically inspired engineering," *Annals of Biomedical Engineering*, 2010.

81. Hall, M. S., R. Long, C. Y. Hui, and M. Wu, "Mapping three-dimensional stress and strain fields within a soft hydrogel using a fluorescence microscope," *Biophysical Journal*, 2012.

82. Wong, V. W., S. Akaishi, M. T. Longaker, and G. C. Gurtner, "Pushing back: Wound mechanotransduction in repair and regeneration," *Journal of Investigative Dermatology*, 2011.

83. Brown, A. E., and D. E. Discher, "Conformational changes and signaling in cell and matrix physics," *Current Biology*, 2009.

84. Cohen, L., and J.-L. Guan, "Mechanisms of focal adhesion kinase regulation," *Current Cancer Drug Targets*, 2005.

85. Poole, K., M. Moroni, and G. R. Lewin, "Sensory mechanotransduction at membrane-matrix interfaces," *Pflugers Archiv European Journal of Physiology*, 2014.

86. Geiger, B., and K. M. Yamada, "Molecular architecture and function of matrix adhesions," *Cold Spring Harbor Perspectives in Biology*, 2011.

87. Legate, K. R., S. A. Wickstrom, and R. Fassler, "Genetic and cell biological analysis of integrin outside-in signaling," *Genes and Development*, 2009.

88. Shih, V. Y. R., K. F. Tseng, H. Y. Lai, C. H. Lin, and O. K. Lee, "Matrix stiffness regulation of integrin-mediated mechanotransduction during osteogenic differentiation of human mesenchymal stem cells," *Journal of Bone and Mineral Research*, 2011.

89. Du, J., X. Chen, X. Liang, G. Zhang, J. Xu, L. He, Q. Zhan, X. Q. Feng, S. Chien, and C. Yang, "Integrin activation and internalization on soft ecm as a mechanism of induction of stem cell differentiation by ecm elasticity," *Proceedings of the National Academy of Sciences of the United States of America*, 2011.

90. Carpenter, D., and S. Ayrapetyan, *Biological Effects of Electric and Magnetic Fields. Vol I*, Vol. 1, Elsevier Ltd., 1994.

91. Wood, C. G., "Wireless radio: A brief history," *Choice*, Vol. 34, no. 5, p. 814, 1997.

92. "World health organization | electromagnetic fields and public health," 2002. [Online; accessed 2020-12-30].

93. Wijngaarden, E., D. Savitz, R. Kleckner, J. Cai, and D. Loomis, "Exposure to electromagnetic fields and suicide among electric utility workers: a nested case-control study," *The Western Journal of Medicine*, Vol. 173, no. 2, pp. 94–100, 2000.

94. Zhou, H., G. Chen, C. Chen, Y. Yu, and Z. Xu, "Association between extremely low-frequency electromagnetic fields occupations and amyotrophic lateral sclerosis: A meta-analysis," *PLoS ONE*, 2012.

95. Saliev, T., Z. Mustapova, G. Kulsharova, D. Bulanin, and S. Mikhalovsky, "Therapeutic potential of electromagnetic fields for tissue engineering and wound healing," *Cell Proliferation*, Vol. 47, no. 6, pp. 485–493, 2014.

96. Ma, Q., C. Chen, P. Deng, G. Zhu, M. Lin, L. Zhang, S. Xu, M. He, Y. Lu, W. Duan, H. Pi, Z. Cao, L. Pei, M. Li, C. Liu, Y. Zhang, M. Zhong, Z. Zhou, and Z. Yu, "Extremely low-frequency electromagnetic fields promote in vitro neuronal differentiation and neurite outgrowth of embryonic neural stem cells via up-regulating trpc1," *Plos One*, Vol. 11, no. 3, p. e0150923, 2016.

97. Kim, H.-J., J. Jung, J.-H. Park, J.-H. Kim, K.-N. Ko, and C.-W. Kim, "Extremely low-frequency electromagnetic fields induce neural differentiation in bone marrow derived mesenchymal stem cells.," *Experimental Biology and Medicine (Maywood, N.J.)*, Vol. 238, pp. 923–31, 2013.

98. Baek, S., X. Quan, S. Kim, C. Lengner, J. K. Park, and J. Kim, "Electromagnetic fields mediate efficient cell reprogramming into a pluripotent state," *ACS Nano*, Vol. 8, no. 10, pp. 10125–10138, 2014.

99. Fanelli, C., S. Coppola, R. Barone, C. Colussi, G. Gualandi, P. Volpe, and L. Ghibelli, "Magnetic fields increase cell survival by inhibiting apoptosis via modulation of ca2+ influx.," *The FASEB Journal*, Vol. 13, no. 1, pp. 95–102, 1999.

100. Walleczek, J., "Electromagnetic field effects on cells of the immune system: the role of calcium signalling," *Faseb*, Vol. 6, pp. 3177–3185, 1992.

101. Karabakhtsian, R., N. Broude, N. Shalts, S. Kochlatyia, R. Goodman, and A. S. Henderson, "Calcium is necessary in the cell response to em fields," *FEBS Letters*, Vol. 349, no. 1, pp. 1–6, 1994.

102. Morgado-Valle, C., L. Verdugo-Diaz, D. E. Garcia, C. Morales-Orozco, and R. Drucker-Colin, "The role of voltage-gated ca2+ channels in neurite growth of cultured chromaffin cells induced by extremely low frequency (elf) magnetic field stimulation," *Cell Tissue Research*, Vol. 291, no. 2, pp. 217–230, 1998.

103. Zhou, J., G. Yao, J. Zhang, and Z. Chang, "Creb dna binding activation by a 50-hz magnetic field in hl60 cells is dependent on extra- and intracellular ca2+ but not pka, pkc, erk, or p38 mapk," *Biochemical and Biophysical Research Communications*, Vol. 296, no. 4, pp. 1013–1018, 2002.

104. Manikonda, P. K., P. Rajendra, D. Devendranath, B. Gunasekaran, Channakeshava, R. S. S. Aradhya, R. B. Sashidhar, and C. Subramanyam, "Influence of extremely low frequency magnetic fields on ca2+ signaling and nmda receptor functions in rat hippocampus," *Neuroscience Letters*, Vol. 413, no. 2, pp. 145–149, 2007.

105. Lisi, A., M. Ledda, E. Rosola, D. Pozzi, E. D'Emilia, L. Giuliani, A. Foletti, A. Modesti, S. J. Morris, and S. Grimaldi, "Extremely low frequency electromagnetic field exposure promotes differentiation of pituitary corticotrope-derived att20 d16v cells," *Bioelectromagnetics*, Vol. 27, no. 8, pp. 641–651, 2006.

106. Sun, Z.-C., J.-L. Ge, B. Guo, J. Guo, M. Hao, Y.-C. Wu, Y.-A. Lin, T. La, P.-T. Yao, Y.-A. Mei, Y. Feng, and L. Xue, "Extremely low frequency electromagnetic fields facilitate vesicle endocytosis by increasing presynaptic calcium channel expression at a central synapse," *Nature Publishing Group*, no. February, pp. 1–11, 2016.

107. Zhang, X., X. Liu, L. Pan, and I. Lee, "Magnetic fields at extremely low-frequency (50 hz, 0.8 mt) can induce the uptake of intracellular calcium levels in osteoblasts," *Biochemical and Biophysical Research Communications*, 2010.

108. Barbier, E., B. Dufy, and B. Veyret, "Stimulation of ca2+ influx in rat pituitary cells under exposure to a 50 hz magnetic field," *Bioelectromagnetics*, 1996.

109. Lai, H., "Exposure to static and extremely-low frequency electromagnetic fields and cellular free radicals," *Electromagnetic Biology and Medicine*, 2019.

110. Gobba, F., D. Malagoli, and E. Ottaviani, "Effects of 50 hz magnetic fields on fmlp-induced shape changes in invertebrate immunocytes: The role of calcium ion channels," *Bioelectromagnetics*, 2003.

111. Piacentini, R., C. Ripoli, D. Mezzogori, G. B. Azzena, and C. Grassi, "Extremely low-freauency electromagnetic fields promote in vitro neurogenesis via upregulation of cav1-channel activity," *Journal of Cellular Physiology*, 2008.

112. Grassi, C., M. D'Ascenzo, A. Torsello, G. Martinotti, F. Wolf, A. Cittadini, and G. B. Azzena, "Effects of 50 hz electromagnetic fields on voltage-gated ca2+ channels and their role in modulation of neuroendocrine cell proliferation and death," *Cell Calcium*, 2004.

113. Huang, C. Y., C. W. Chang, C. R. Chen, C. Y. Chuang, C. S. Chiang, W. Y. Shu, T. C. Fan, and I. C. Hsu, "Extremely low-frequency electromagnetic fields cause g1 phase arrest through the activation of the atm-chk2-p21 pathway," *PLoS ONE*, 2014.

114. Ehnert, S., A. K. Fentz, A. Schreiner, J. Birk, B. Wilbrand, P. Ziegler, M. K. Reumann, H. Wang, K. Falldorf, and A. K. Nussler, "Extremely low frequency pulsed electromagnetic fields cause antioxidative defense mechanisms in human osteoblasts via induction of â¢o2- and h2o2," *Scientific Reports*, 2017.

115. Cho, H., Y. K. Seo, H. H. Yoon, S. C. Kim, S. M. Kim, K. Y. Song, and J. K. Park, "Neural stimulation on human bone marrow-derived mesenchymal stem cells by extremely low frequency electromagnetic fields," *Biotechnol Prog*, Vol. 28, no. 5, pp. 1329–1335, 2012.

116. Park, J.-E., Y.-K. Seo, H.-H. Yoon, C.-W. Kim, J.-K. Park, and S. Jeon, "Electromagnetic fields induce neural differentiation of human bone marrow derived mesenchymal stem cells via ros mediated egfr activation.," *Neurochemistry International*, Vol. 62, no. 4, pp. 418–24, 2013.

117. Sun, W., Y. Gan, Y. Fu, D. Lu, and H. Chiang, "An incoherent magnetic field inhibited egf receptor clustering and phosphorylation induced by a 50-hz magnetic field in cultured fl cells," *Cellular Physiology and Biochemistry*, 2008.

118. Seals, D. F., and S. A. Courtneidge, "The adams family of metalloproteases: Multidomain proteins with multiple functions," *Genes and Development*, Vol. 17, no. 1, pp. 7–30, 2003.

119. Patruno, A., A. Ferrone, E. Costantini, S. Franceschelli, M. Pesce, L. Speranza, P. Amerio, C. D'Angelo, M. Felaco, A. Grilli, and M. Reale, "Extremely low-frequency electromagnetic fields accelerates wound healing modulating mmp-9 and inflammatory cytokines," *Cell Proliferation*, 2018.

120. Stork, C. J., and V. Y. Li, "Intracellular zinc elevation measured with a "calcium-specific" indicator during ischemia and reperfusion in rat hippocampus: a question on calcium overload.," *The Journal of Neuroscience*, Vol. 26, no. 41, pp. 10430–7, 2006.

121. Sensi, S. L., P. Paoletti, A. I. Bush, and I. Sekler, "Zinc in the physiology and pathology of the cns.," *Nature Reviews. Neuroscience*, Vol. 10, no. 11, pp. 780–791, 2009.

122. Fujikawa, K., R. Fukumori, S. Nakamura, T. Kutsukake, T. Takarada, and Y. Yoneda, "Potential interactions of calcium-sensitive reagents with zinc ion in different cultured cells," *PLoS ONE*, 2015.

123. Yamasaki, S., K. Sakata-Sogawa, A. Hasegawa, T. Suzuki, K. Kabu, E. Sato, T. Kurosaki, S. Yamashita, M. Tokunaga, K. Nishida, and T. Hirano, "Zinc is a novel intracellular second messenger," *Journal of Cell Biology*, 2007.

124. Wu, Z. Z., Z. W. Wang, L. G. Zhang, Z. X. An, D. H. Zhong, Q. P. Huang, M. R. Luo, Y. J. Liao, L. Jin, C. Z. Li, and W. S. Kisaalita, "Responsiveness of voltage-gated calcium channels in sh-sy5y human neuroblastoma cells on quasi-three-dimensional micropatterns formed with poly (l-lactic acid)," *International Journal of Nanomedicine*, 2012.

125. Garland, S. P., C. T. McKee, Y. R. Chang, V. K. Raghunathan, P. Russell, and C. J. Murphy, "A cell culture substrate with biologically relevant size-scale topography and compliance of the basement membrane," *Langmuir*, 2014.

126. Cui, M., H. Ge, H. Zhao, Y. Zou, Y. Chen, and H. Feng, "Electromagnetic fields for the regulation of neural stem cells," *Stem Cells International*, Vol. 2017, 2017.

127. Mendez, I., A. Dagher, M. Hong, P. Gaudet, S. Weerasinghe, V. McAlister, D. King, J. Desrosiers, S. Darvesh, T. Acorn, and H. Robertson, "Simultaneous intrastriatal and intranigral fetal dopaminergic grafts in patients with parkinson disease: a pilot study. report of three cases," *J.Neurosurg.*, 2002.

128. Baghbaderani, B. A., K. Mukhida, A. Sen, M. S. Kallos, M. Hong, I. Mendez, and L. A. Behie, "Bioreactor expansion of human neural precursor cells in serum-free media retains neurogenic potential," *Biotechnology and Bioengineering*, 2010.

129. Teixeira, F. G., K. M. Panchalingam, S. I. Anjo, B. Manadas, R. Pereira, N. Sousa, A. J. Salgado, and L. A. Behie, "Do hypoxia/normoxia culturing conditions change the neuroregulatory profile of wharton jelly mesenchymal stem cell secretome?," *Stem Cell Research and Therapy*, 2015.

130. Jantas, D., and W. Lason, "Protective effect of memantine against doxorubicin toxicity in primary neuronal cell cultures: Influence a development stage," *Neurotoxicity Research*, 2009.

131. Teixeira, F. G., K. M. Panchalingam, R. Assuncao-Silva, S. C. Serra, B. Mendes-Pinheiro, P. Patricio, S. Jung, S. I. Anjo, B. Manadas, L. Pinto, N. Sousa, L. A. Behie, and A. J. Salgado, "Modulation of the mesenchymal stem cell secretome using computer-controlled bioreactors: Impact on neuronal cell proliferation, survival and differentiation," *Scientific Reports*, 2016.

132. Jacob, M., M. Unser, J.-C. Sarria, E. Meijering, H. Hirling, and P. Steiner, "Design and validation of a tool for neurite tracing and analysis in fluorescence microscopy images," *Cytometry*, Vol. 58A, no. 2, pp. 167–176, 2004.

133. Consales, C., C. Merla, C. Marino, and B. Benassi, "Electromagnetic fields, oxidative stress, and neurodegeneration," *International Journal of Cell Biology*, 2012.

134. Liu, X., H. Zuo, D. Wang, R. Peng, T. Song, S. Wang, X. Xu, Y. Gao, Y. Li, S. Wang, L. Wang, and L. Zhao, "Improvement of spatial memory disorder and hippocampal damage by exposure to electromagnetic fields in an alzheimer's disease rat model," *PLoS ONE*, Vol. 10, no. 5, 2015.

135. Arendash, G. W., J. Sanchez-Ramos, T. Mori, M. Mamcarz, X. Lin, M. Runfeldt, L. Wang, G. Zhang, V. Sava, J. Tan, and C. Cao, "Electromagnetic field treatment protects against and reverses cognitive impairment in alzheimer's disease mice.," *Journal of Alzheimer's disease : JAD*, Vol. 19, no. 1, pp. 191–210, 2010.

136. Hu, Y., J. Lai, B. Wan, X. Liu, Y. Zhang, J. Zhang, D. Sun, G. Ruan, E. Liu, G. P. Liu, C. Chen, and D. W. Wang, "Long-term exposure to elf-mf ameliorates cognitive deficits and attenuates tau hyperphosphorylation in 3xtg ad mice," *NeuroToxicology*, 2016.

137. Ma, Q., P. Deng, G. Zhu, C. Liu, L. Zhang, Z. Zhou, X. Luo, M. Li, M. Zhong, Z. Yu, C. Chen, and Y. Zhang, "Extremely low-frequency electromagnetic fields affect transcript levels of neuronal differentiation-related genes in embryonic neural stem cells," *PLoS ONE*, Vol. 9, no. 3, 2014.

138. Cuccurazzu, B., L. Leone, M. V. Podda, R. Piacentini, E. Riccardi, C. Ripoli, G. B. Azzena, and C. Grassi, "Exposure to extremely low-frequency (50hz) electromagnetic fields enhances adult hippocampal neurogenesis in c57bl/6 mice," *Experimental Neurology*, Vol. 226, no. 1, pp. 173–182, 2010.

139. Papadia, S., and G. E. Hardingham, "The dichotomy of nmda receptor signaling," *Neuroscientist*, 2007.

140. Yoneyama, M., N. Nakamichi, M. Fukui, T. Kitayama, D. D. Georgiev, J. O. Makanga, N. Nakamura, H. Taniura, and Y. Yoneda, "Promotion of neuronal differentiation through activation of n-methyl-d-aspartate receptors transiently expressed by undifferentiated neural progenitor cells in fetal rat neocortex," *Journal of Neuroscience Research*, 2008.

141. Joo, J.-Y., B.-W. Kim, J.-S. Lee, J.-Y. Park, S. Kim, Y.-J. Yun, S.-H. Lee, S.-H. Lee, H. Rhim, and H. Son, "Activation of nmda receptors increases proliferation and differentiation of hippocampal neural progenitor cells," *Journal of Cell Science*, Vol. 120, no. 8, pp. 1358–1370, 2007.

142. Jansson, L. C., and K. E. Akerman, "The role of glutamate and its receptors in the proliferation, migration, differentiation and survival of neural progenitor cells," *Journal of Neural Transmission*, 2014.

143. Tang, S.-J., X.-L. Yang, B. Li, W. Zhang, X.-Z. Wan, L. Zhong, and Y.-C. Li, "Activation of nmda receptors upregulates a disintegrin and metalloproteinase 10 via a wnt/mapk signaling pathway," *Journal of Neuroscience*, 2012.

144. Sanalkumar, R., S. Vidyanand, C. Lalitha Indulekha, and J. James, "Neuronal vs. glial fate of embryonic stem cell-derived neural progenitors (es-nps) is determined by fgf2/egf during proliferation," *Journal of Molecular Neuroscience*, 2010.

145. Ayanlaja, A. A., Y. Xiong, Y. Gao, G. Ji, C. Tang, Z. Abdikani Abdullah, and D. Gao, "Distinct features of doublecortin as a marker of neuronal migration and its implications in cancer cell mobility.," *Frontiers in Molecular Neuroscience*, 2017.

146. Seong, Y., J. Moon, and J. Kim, "Egr1 mediated the neuronal differentiation induced by extremely low-frequency electromagnetic fields," *Life Sciences*, Vol. 102, no. 1, pp. 16–27, 2014.

147. Parsons, C. G., and K. Gilling, "Memantine as an example of a fast, voltage-dependent, open channel n-methyl-d-aspartate receptor blocker," in *Patch-Clamp Methods and Protocols*, 2007.

148. Johnson, J. W., and S. E. Kotermanski, "Mechanism of action of memantine," *Current Opinion in Pharmacology*, 2006.

149. Lerea, L., L. Butler, and J. McNamara, "Nmda and non-nmda receptor-mediated increase of c-fos mrna in dentate gyrus neurons involves calcium influx via different routes," *The Journal of Neuroscience*, 2018.

150. Pearce, I. A., M. A. Cambray-Deakin, and R. D. Burgoyne, "Glutamate acting on nmda receptors stimulates neurite outgrowth from cerebellar granule cells," *FEBS Letters*, 1987.

151. "Suppression of neurite outgrowth of primary cultured hippocampal neurons is involved in impairment of glutamate metabolism and nmda receptor function caused by nanoparticulate tio2," *Biomaterials*.

152. Cambray-Deakin, M., and B. R.D., "Regulation of neurite outgrowth from cerebellar granule cells in culture: Nmda receptors and protein kinase c," in *Excitatory Amino Acids and Neuronal Plasticity. Advances in Experimental Medicine and Biology*, Springer, Boston, MA, 1990.

153. De Bartolomeis, A., C. Sarappa, E. F. Buonaguro, F. Marmo, A. Eramo, C. Tomasetti, and F. Iasevoli, "Different effects of the nmda receptor antagonists ketamine, mk-801, and memantine on postsynaptic density transcripts and their topography: Role of homer signaling, and implications for novel antipsychotic and pro-cognitive targets in psychosis," *Progress in Neuro-Psychopharmacology and Biological Psychiatry*, 2013.

154. Sivandzade, F., A. Bhalerao, and L. Cucullo, "Analysis of the mitochondrial membrane potential using the cationic jc-1 dye as a sensitive fluorescent probe," *BIO-PROTOCOL*, 2019.

155. Gerasimenko, V. J., O. H. Petersen, and V. O. Gerasimenko, "Monitoring of intra-er free ca2+," *Wiley Interdisciplinary Reviews: Membrane Transport and Signaling*, 2014.

156. Wang, H., and X. Zhang, "Magnetic fields and reactive oxygen species," *International Journal of Molecular Sciences*, 2017.

157. Suski, J., M. Lebiedzinska, M. Bonora, P. Pinton, J. Duszynski, and M. R. Wieckowski, "Relation between mitochondrial membrane potential and ros formation," in *Methods in Molecular Biology*, 2018.

158. Qian, C., and R. A. Colvin, "Zinc flexes its muscle: Correcting a novel analysis of calcium for zinc interference uncovers a method to measure zinc," *The Journal of General Physiology*, Vol. 147, no. 1, pp. 95–102, 2016.

159. Venkatachalam, K., and C. Montell, "Trp channels," *Annual Review of Biochemistry*, 2007.

160. Park, S. J., S. H. Min, H. W. Kang, and J. H. Lee, "Differential zinc permeation and blockade of l-type ca2+ channel isoforms cav1.2 and cav1.3," *Biochimica et Biophysica Acta - Biomembranes*, 2015.

161. Inoue, K., Z. O'Bryant, and Z.-G. Xiong, "Zinc-permeable ion channels: Effects on intracellular zinc dynamics and potential physiological/pathophysiological significance," *Current Medicinal Chemistry*, Vol. 22, no. 10, pp. 1248–1257, 2015.

162. Lievremont, J. P., G. S. Bird, and J. W. Putney, "Mechanism of inhibition of trpc cation channels by 2- aminoethoxydiphenylborane," *Molecular Pharmacology*, 2005.

163. Naziroglu, M., C. Ozgul, O. Celik, B. Cig, and E. Sozbir, "Aminoethoxydiphenyl borate and flufenamic acid inhibit ca2+ influx through trpm2 channels in rat dorsal root ganglion neurons activated by adp-ribose and rotenone," *Journal of Membrane Biology*, 2011.

164. Chokshi, R., P. Fruasaha, and J. A. Kozak, "2-aminoethyl diphenyl borinate (2-apb) inhibits trpm7 channels through an intracellular acidification mechanism," *Channels*, 2012.

165. Bencze, M., M. Behuliak, A. Vavrinova, and J. Zicha, "Broad-range trp channel inhibitors (2-apb, flufenamic acid, skf-96365) affect differently contraction of resistance and conduit femoral arteries of rat," *European Journal of Pharmacology*, 2015.

166. Ortner, N. J., and J. Striessnig, "L-type calcium channels as drug targets in cns disorders," *Channels*, 2016.

167. Huguenard, J. R., "Block of t -type ca2+ channels is an important action of succinimide antiabsence drugs," *Epilepsy Currents*, 2002.

168. Sutton, K. G., D. J. Martin, R. D. Pinnock, K. Lee, and R. H. Scott, "Gabapentin inhibits high-threshold calcium channel currents in cultured rat dorsal root ganglion neurones," *British Journal of Pharmacology*, 2002.

169. Song, X., M. O. Jensen, V. Jogini, R. A. Stein, C. H. Lee, H. S. McHaourab, D. E. Shaw, and E. Gouaux, "Mechanism of nmda receptor channel block by mk-801 and memantine," *Nature*, Vol. 556, no. 7702, pp. 515–519, 2018.

170. Adler, M., R. E. Dinterman, and R. W. Wannemacher, "Protection by the heavy metal chelator n,n,n',n'-tetrakis (2- pyridylmethyl)ethylenediamine (tpen) against the lethal action of botulinum neurotoxin a and b," *Toxicon*, 1997.

171. "Pan biotech dmem/f12 composition," 0. [Online; accessed 2020-11-25].

172. Ortyn, W. E., B. E. Hall, T. C. George, K. Frost, D. A. Basiji, D. J. Perry, C. A. Zimmerman, D. Coder, and P. J. Morrissey, "Sensitivity measurement and compensation in spectral imaging," *Cytometry Part A*, 2006.

173. Wei, M., Y. Zhou, A. Sun, G. Ma, L. He, L. Zhou, S. Zhang, J. Liu, S. L. Zhang, D. L. Gill, and Y. Wang, "Molecular mechanisms underlying inhibition of stim1-orai1-mediated ca2+ entry induced by 2-aminoethoxydiphenyl borate," *Pflugers Archiv European Journal of Physiology*, 2016.

174. Kovacs, G., N. Montalbetti, M. C. Franz, S. Graeter, A. Simonin, and M. A. Hediger, "Human trpv5 and trpv6: Key players in cadmium and zinc toxicity," *Cell Calcium*, 2013.

175. Himmel, N. J., and D. N. Cox, "Transient receptor potential channels: current perspectives on evolution, structure, function and nomenclature," *Proceedings. Biological sciences*, 2020.

176. Legrand, C., J. M. Merlini, C. de Senarclens-BezenÃ§on, and S. Michlig, "New natural agonists of the transient receptor potential ankyrin 1 (trpa1) channel," *Scientific Reports*, Vol. 10, no. 1, pp. 1–10, 2020.

177. Peng, S., M. S. Grace, A. B. Gondin, J. S. Retamal, L. Dill, W. Darby, N. W. Bunnett, F. C. Abogadie, S. E. Carbone, T. Tigani, T. P. Davis, D. P. Poole, N. A. Veldhuis, and P. McIntyre, "The transient receptor potential vanilloid 4 (trpv4) ion channel mediates protease activated receptor 1 (par1)-induced vascular hyperpermeability," *Laboratory Investigation*, 2020.

178. Kimura, T., and T. Kambe, "The functions of metallothionein and zip and znt transporters: An overview and perspective," *International Journal of Molecular Sciences*, 2016.